NACA

RESEARCH MEMORANDUM

WIND-TUNNEL INVESTIGATION AT MACH NUMBERS OF 2.0 AND 2.9 OF SEVERAL CONFIGURATIONS OF A SUPERSONIC RAM-JET TEST VEHICLE

By J. Richard Spahr and Robert A. Robinson

Ames Aeronautical Laboratory
Moffett Field, Calif.

NATIONAL ADVISORY COMMITTEE
FOR AERONAUTICS

WASHINGTON

August 18, 1950

E R R A T A

NACA RM A50C20

WIND-TUNNEL INVESTIGATION AT MACH NUMBERS OF 2.0 AND 2.9 OF SEVERAL CONFIGURATIONS OF A SUPERSONIC RAM-JET TEST VEHICLE

By J. Richard Spahr and Robert A. Robinson

The following changes should be noted:

1. Page 1, last line:

   Insert "at an angle of attack of 0°" after "effect."

2. Page 3, first sentence under NOTATION:

   Change sentence to "All forces are referred to the wind axes and moments to the stability axes with the origin at the moment reference point."

3. Page 15, line 33:

   Insert "at an angle of attack of 0°" after "adverse."

4. Page 16, line 26:

   Add "at an angle of attack of 0°" after "effect."

5. Table II:

   The C_l arrow should be centered about the longitudinal body axis in the plan view and about the streamwise axis in the side view.

NACA-Langley - 11-21-50 - 425

NATIONAL ADVISORY COMMITTEE FOR AERONAUTICS

RESEARCH MEMORANDUM

WIND-TUNNEL INVESTIGATION AT MACH NUMBERS OF 2.0 AND 2.9 OF SEVERAL CONFIGURATIONS OF A SUPERSONIC RAM-JET TEST VEHICLE

By J. Richard Spahr and Robert A. Robinson

SUMMARY

Wind-tunnel tests were conducted at Mach numbers of 2.0 and 2.9 to investigate the aerodynamic characteristics of several configurations of a supersonic ram-jet test vehicle. Three low-aspect-ratio wing configurations, with the ram-jet engine located forward and below the wing, were tested in pitch at a Mach number of 2.0. These configurations consisted of a rectangular wing between two bodies with triangular tail surfaces, a 72° swept-back untapered wing between two bodies and tail surfaces identical to those for the rectangular-wing configuration, and a triangular wing with 72° leading-edge sweepback in combination with a central body having a triangular vertical fin. Tests of a fourth model, a triangular-wing configuration similar to the third configuration but with the engine above and to the rear of the wing, were performed in both pitch and sideslip at Mach numbers of 2.0 and 2.9. Force tests of the ram-jet engine and of the engine-strut-body combination for this configuration were also made in pitch at these two Mach numbers.

It was found that of the various configurations tested the triangular-wing arrangement exhibited the best lift-drag ratio throughout the operating lift-coefficient range. Relocation of the ram-jet engine from the front to the rear of the triangular-wing configuration, as required by dynamic-lateral-stability considerations, resulted in a slight adverse effect on the lift-drag ratio.

All the configurations investigated were longitudinally stable with respect to the 25-percent point of the mean aerodynamic chord. The configuration with the engine at the rear was found to be directionally stable at a Mach number of 2.0 but exhibited a slight negative dihedral effect, despite the relatively large geometric dihedral (15°).

Values for the theoretical lift and pitching-moment characteristics $dC_L/d\alpha$ and dC_m/dC_L of the four configurations have been computed through the use of linear theories, and comparisons with the corresponding experimental results are presented. The experimental and theoretical results are in close agreement in those cases for which the effects of viscosity and of interference between the engine-inlet and wing-body flow fields are expected to be small.

Static-pressure surveys of the flow field above the body alone indicated that flow conditions at the position of the inlet of the rearward located engine were very close to free-stream conditions at Mach numbers of 2.0 and 2.9 and at angles of attack of 0° and 5°.

INTRODUCTION

An increasing need exists for information on the performance characteristics of supersonic ram-jet propulsion systems under full-scale operating conditions. One means for obtaining such information is through the use of a flight-test vehicle propelled by the test engine itself. An aircraft designed specifically for this purpose and designated as the A-1 supersonic ram-jet test vehicle is currently under development for the U. S. Air Force by the Lockheed Aircraft Corporation. This test vehicle is designed to operate at relatively low lift coefficients over a range of Mach numbers from 1.7 to 3.0 and at altitudes between sea level and 80,000 feet. The optimum configuration for such a test vehicle is one which would give the best flight endurance at these operating conditions. Since endurance is a function of the ratio of lift to drag at a given gross weight, the optimum configuration would possess the best lift-drag ratio over the operating range of lift coefficients. Other necessary requirements for an acceptable configuration are that it exhibit static and dynamic longitudinal and lateral stability and that sufficient longitudinal control be available to effect trim at all test conditions.

Three preliminary configurations for a ram-jet test vehicle were developed, each having a low-aspect-ratio wing of different plan form. The ram-jet engine was mounted on a strut below and at the front of the test vehicle so that the engine inlet would operate at free-stream conditions. These three configurations (figs. 1 to 3 and table I) consisted of (1) a rectangular wing between two bodies with triangular horizontal and vertical tail surfaces, (2) a 72° swept-back untapered wing between two bodies and tail surfaces identical to those of (1), and (3) a triangular wing with 72° leading-edge sweepback in combination with a single body having a triangular vertical fin. Tests were conducted in the Ames 1- by 3-foot supersonic wind tunnel No. 2 at a Mach number of 2.0 for the primary purpose of providing data from which the best of these three configurations could be selected.

Subsequent theoretical and experimental studies conducted by the Lockheed Aircraft Corporation indicated that the triangular-wing configuration would exhibit unsatisfactory lateral dynamic-stability characteristics. Consequently, a fourth configuration (fig. 4 and table I) was evolved by a relocation of the ram-jet engine to the rear and above the test vehicle in an attempt to improve these dynamic-stability characteristics. This configuration was tested in the 1- by 3-foot wind tunnel at Mach numbers of 2.0 and 2.9 to determine the aerodynamic characteristics of the model and its components in pitch and the characteristics of the complete configuration in sideslip. Since the engine inlet for the fourth configuration was located within the velocity field of the body, pressure surveys in the vicinity of the inlet location were conducted at two angles of attack and at both Mach numbers to determine the deviation of the inlet conditions from those existing in the free stream.

These tests were performed at the request of the Air Materiel Command, U. S. Air Force.

NOTATION

All forces and moments are referred to wind axes with the origin at the moment reference point. (See table II for directions of forces and moments, and see figs. 1 to 4 for location of moment reference point.)

b wing span

c wing chord parallel to plane of symmetry

$\bar{c}$ mean aerodynamic chord $\left(\dfrac{\int_0^{b/2} c^2\,dy}{\int_0^{b/2} c\,dy}\right)$

C_D drag coefficient $\left(\dfrac{\text{drag}}{qS}\right)$

ΔC_D rise in drag coefficient above minimum $\left(C_D - C_{D_{min}}\right)$

$C_{D_{min}}$ minimum drag coefficient

C_l rolling-moment coefficient $\left(\dfrac{\text{rolling moment}}{qSb}\right)$

C_L lift coefficient $\left(\dfrac{\text{lift}}{qS}\right)$

C_m pitching-moment coefficient $\left(\dfrac{\text{pitching moment}}{qS\bar{c}}\right)$

C_n yawing-moment coefficient $\left(\dfrac{\text{yawing moment}}{qSb}\right)$

C_Y side-force coefficient $\left(\frac{\text{side force}}{qS}\right)$

M Mach number

p local static pressure

p_o free-stream static pressure

P pressure coefficient $\left(\frac{p-p_o}{q}\right)$

q dynamic pressure

R Reynolds number based on mean aerodynamic chord

S total wing area (formed by the leading and trailing edges extended to the body center lines)

x,y,z longitudinal, lateral, and normal coordinates with the x axis corresponding to the wing center line

α angle of attack

β angle of sideslip

δ elevon deflection

Subscripts

L=0 value of zero lift

av average value

APPARATUS

Wind Tunnel and Balance

The investigation was conducted in the Ames 1- by 3-foot supersonic wind tunnel No. 2, which is an intermittent-operation, nonreturn, variable-pressure wind tunnel. The compressed-air supply is obtained from the Ames 12-foot pressure wind tunnel and is expanded through the 1- by 3-foot tunnel to atmospheric pressure. The total-pressure level, and hence the Reynolds number, is controlled by means of a throttling valve. The 1- by 3-foot wind tunnel is equipped with a variable Mach number nozzle with

a rectangular test section 1 foot wide by approximately 3 feet high. The Mach number can be varied from about 1.2 to 3.4 by changing the shape of the flexible steel plates which form the upper and lower walls of the nozzle.

The strain-gage balance and other instrumentation used in these tests were essentially the same as those employed in the Ames 1- by 3-foot supersonic wind tunnel No. 1. (See reference 1.) In the present investigation, pitching or yawing moments were measured by means of strain gages mounted on the model supporting sting. Strain gages were also incorporated in the balance for the measurement of the rolling moment about the balance axis. A drawing of the strain-gage balance and model support is given in figure 5.

Models and Supports

The four different configurations employed in the investigation are designated as follows:

Configuration I - Rectangular wing between two bodies with triangular horizontal and vertical tail surfaces and having the ram-jet engine located below and at the front of the model (fig. 1).

Configuration II - A 72° swept-back untapered wing between two bodies with tail surfaces identical to those of configuration I and having the ram-jet engine located below and at the front of the model (fig. 2).

Configuration III - Triangular wing with 72° leading-edge sweepback in combination with a single body and having the ram-jet engine located below and at the front of the model (fig. 3).

Configuration IV - Triangular wing with 72° leading-edge sweepback in combination with a single body and having the ram-jet engine located above and at the rear of the model (fig. 4).

The geometric characteristics of the four configurations are tabulated in table I. All wing and tail surfaces were of biconvex section. The triangular wings of configurations III and IV incorporated constant-chord, full-span, trailing-edge control surfaces for longitudinal and lateral control. Deflection of these controls on the model was obtained by bending the surfaces along an undercut on both upper and lower surfaces at the hinge-line location. After the control surfaces were bent in a jig to the desired deflection, the grooves were filled with soft solder to provide a fairing along the hinge line.

The ram-jet engine model (fig. 6) used with all four configurations provided for internal flow through the engine and incorporated an annular nose inlet with an external double-shock diffuser. The cross-sectional

area of the duct through the engine increased from the minimum at the inlet to a maximum value within the engine, followed by a decrease to a second throat near the exit. The distribution of area through the duct relative to the inlet area is shown in figure 6(b). The ratio of the exit-throat area to the inlet area was 1.31 for all tests.

All the models were supported on a sting connected to the rear of the engine inner body, as shown in figures 5 and 7. For the pitch tests the models were mounted in an inverted position (fig. 7(a)), and for the sideslip tests with the plane of the wing vertical (fig. 7(b)). The sting support was shielded from aerodynamic forces by a shroud that extended to within a small distance from the engine base. Static-pressure orifices in the sting adjacent to the base of the inner body permitted the measurement of the pressure acting on the base.

The body of revolution used in the pressure-survey tests was similar to that for configurations III and IV but was of slightly greater fineness ratio. Dimensions of the model are given in figure 8(a). Pressure orifices were located longitudinally along the upper surface of the model in the vertical plane of symmetry for the measurement of the surface pressures. The pressure-survey apparatus used in the measurement of the static pressure above the model surface consisted of a static-pressure probe, sting supported on a traversing device, which could be moved in a vertical plane in directions either parallel or normal to the model axis. The static-pressure probe was a slender cylindrical body with a pointed nose and having the orifice holes located near the base of the probe where the static pressure is theoretically very nearly equal to the free-stream pressure. A photograph of the model, with the survey probe installed on the traversing device, is shown in figure 8(b).

TESTS AND METHODS

Force Tests

In the first phase of the investigation, configurations I, II, and III were tested in pitch with control surfaces neutral at a Mach number of 2.0. Lift, drag, and pitching moment were measured through an angle-of-attack range of approximately -2° to $+6^\circ$. In the second phase, similar tests of configuration IV, of the engine alone, and of the engine, strut, and body were each performed in pitch at Mach numbers of 2.0 and 2.9. An additional run with the complete configuration having the control surfaces deflected about 1.5° was also made at a Mach number of 2.9. Tests of the model at Mach numbers of both 2.0 and 2.9 with the control surfaces deflected to several angles up to 10° were also planned. However, such tests were precluded as the result of a model-support failure and the consequent model destruction. Tests of configuration IV were conducted in sideslip at a Mach number of 2.0. For these tests, side force, drag, yawing moment, and rolling moment were measured through

an angle range of about -2° to $+6^{\circ}$.

The average Reynolds number per foot for these tests was 10.4 and 13.9×10^6, corresponding to Mach numbers of 2.0 and 2.9, respectively. The angle of inclination of the model relative to horizontal was determined in all cases from the balance-angle setting, the measured forces and moments, and a predetermined spring constant for the balance system. The control-surface deflections were determined from direct optical measurements obtained during testing.

Pressure Surveys

Longitudinal static-pressure surveys were conducted at three locations above the body in the vertical plane of symmetry, at angles of attack of 0° and 5°, and at Mach numbers of 2.0 and 2.9. In addition, pressures were obtained along the body surface for these conditions.

Method of Analysis

All the drag data have been reduced to correspond to a common pressure on the base of the engine inner body equal to the free-stream static pressure. Thus, these data represent the difference between the total drag and the base drag. No attempt was made to evaluate the magnitude of the internal drag of the engine as accurate measurements were not possible. The increment of drag due to internal flow through the engine would be expected to be essentially the same for all configurations tested at a given Mach number. The measured drag was not corrected for the effects of the longitudinal static-pressure gradients in the wind tunnel since these effects were found to be negligible. The local flow inclinations (stream angle) of the wind-tunnel stream with respect to horizontal were taken into account, and all angle-of-attack and sideslip-angle measurements have been corrected for this effect. The model angle of attack (or sideslip) was taken as the algebraic sum of the average stream angle along the model and the model inclination relative to horizontal. With the models supported at the rear of the engine unit, configurations I, II, and III were subjected to possible support-interference effects due to the forward location of the engine relative to the other components. No evaluation of the support interference was made as it is believed that the effect was small.

The static pressures measured in the body-pressure-survey tests have been corrected by the method of superposition for the longitudinal variations of free-stream static pressure in the wind tunnel.

Precision of Results

The accuracy of the experimental results was determined as the square root of the sum of the squares of the component errors due to the uncertainty in each measurement. The following values were obtained for the uncertainty of the force and moment coefficients at a lift (or side force) coefficient of approximately 0.10:

C_L and C_Y	±0.001
C_m and C_n	±.002
C_l	±.0002
C_D	±.001

The uncertainty of the angle-of-attack or angle-of-sideslip measurement is $\pm 0.10^\circ$. The control deflection was measured within $\pm 0.15^\circ$, but varied $\pm 0.40^\circ$ with changes in the model angle of attack. The free-stream Mach number is known within ±0.002, but varied over the length of the model by a maximum of ±0.03 at M = 2.0 and ±0.05 at M = 2.9. The Reynolds number per foot for the investigation varied during a test run by about 0.78×10^6 at both Mach numbers due to the decrease in the wind-tunnel stagnation temperature.

RESULTS

The experimental results for configurations I, II, and III at a Mach number of 2.0 are presented in figure 9 in terms of lift, pitching-moment, and drag coefficients as functions of angle of attack. Figure 10 shows the variation of lift-drag ratio with lift coefficient. The corresponding results for configuration IV at Mach numbers of 2.0 and 2.9, including those for the ram-jet engine and the engine-strut-body combination, are given in figures 11, 12, and 13. All the force and moment coefficients for the model components (figs. 11 and 12) are based on the wing area and mean aerodynamic chord of configuration IV, and the pitching-moment results are referred to the moment reference point of this configuration (fig. 4(d)). It should also be noted that all the aerodynamic coefficients for configurations III and IV are based on a wing area approximately 20 percent greater than that for configurations I and II (see table I); hence, in any comparison of the results between the various configurations, this difference should be taken into account. The results for configuration IV with deflected controls are also given in figure 12. Schlieren photographs of the engine-inlet flow field at two angles of attack and both Mach numbers are shown in figures 14 and 15. The results for configuration IV in sideslip at a Mach number of 2.0 are presented in figure 16 in terms of side-force, yawing-moment, rolling-moment, and drag coefficients as functions of angle of sideslip.

A summary of the results is given in table II in terms of the slopes and intercepts of the experimental curves.

Theoretical values for the lift-curve slope $dC_L/d\alpha$ and the moment-curve slope dC_m/dC_L were computed for the four complete configurations through the use of inviscid linear supersonic-flow theories (references 2 to 8) for wings, bodies, and combinations. For these calculations, experimental values were used for the engine lift and moment characteristics in the absence of an adequate theoretical method. The total lift- and moment-curve slopes were taken as the algebraic sum of the values for the components (wings, bodies, tails, and engine) acting alone, with the addition of the effects of wing-body interaction where possible. No estimates of the angles of attack for zero lift and moment were possible because of the unknown interaction effects between the engine and wing-body flow fields. The theoretical lift and moment curves are given in figures 9, 11, and 12. For purposes of comparison with the experimental lift- and moment-curve slopes these curves are drawn through the values on the experimental curves corresponding to zero lift coefficient. The theoretical results are summarized with the corresponding experimental values in table II.

The results for the survey of the body pressure field are given in figure 17. The corresponding theoretical pressure distributions at 0° angle of attack, computed by the Lockheed Aircraft Corporation through the use of the method of characteristics, are shown for comparison.

DISCUSSION

Configurations I, II, and III

Configuration I.- The results for the rectangular-wing configuration (fig. 9(a)) show that the lift-curve slope is constant throughout the angle-of-attack range and that a small negative lift coefficient is present at zero angle of attack. The pitching-moment curve is also linear throughout the angle-of-attack range and has a negative slope, indicating constant and positive static longitudinal stability relative to the 25-percent point of the mean aerodynamic chord. From figure 9(a) and table II, it is noted that the slopes of these curves $dC_L/d\alpha$ and dC_m/dC_L are in close agreement with the corresponding theoretical results.

The theoretical lift and moment characteristics of this configuration were computed on the assumption that the two-dimensional lift distribution (reference 2) acts on the wing extended to the body axes. The basis for this assumption is that the wing-tip bodies would be expected to prevent a large part of the normal loss in lift at the wing tips. Experimental results of reference 1 indicated that for wing-body combinations in which the wing was relatively large in comparison with the

body, the portion of the wing contained within the body was fully effective in lift with no apparent loss due to wing–body interference effects. The theoretical lift– and moment–curve slopes for the bodies were obtained from the slender–body theory of reference 3. The lift and moment contributions of the tail surfaces were computed by the method of reference 4 on the assumption that the theoretical lift and moment characteristics for the equivalent triangular wing are applicable to that portion of the tail surfaces within the Mach cone originating at the leading edge of the tail–body juncture. (See fig. 1(d).) The vertical fins would be expected to act as end plates and hence would tend to maintain the theoretical load distribution.

The small positive angle of attack for zero lift (fig. 9(a)) is believed to be principally the result of the mutual interaction of the flow fields from the engine and inlet with that of the wing–body combinations. No theoretical prediction of this effect was possible. The agreement between the experimental and theoretical lift and moment results indicates that the interference effects among the various components are compensating or are small in terms of the over–all characteristics of the configuration.

Configuration II.– The results for the swept–back–wing configuration (fig. 9(b)) show that the lift curve is linear up to an angle of attack of about 3° above which a slight increase in slope occurs. This increase may be partially due to the influence of the body and engine lift characteristics which previous experimental and theoretical results have shown to have an increasing lift–curve slope $dC_L/d\alpha$ with increasing angles of attack. (See reference 5.) The small positive angle of attack for zero lift, as in the case of configuration I, is presumably the result of interaction effects between the flow fields of the model components. The pitching–moment curve (fig. 9(b)) indicates positive static longitudinal stability which increases slightly with increasing angle of attack. It is noted that both the lift– and moment–curve slopes are somewhat less than the corresponding theoretical results. (See fig. 9(b) and table II.)

The theoretical lift and moment characteristics of this configuration were computed on the assumption that the basic load distribution for a swept–back wing (reference 6) acts on the wing extended to the body axes since the presence of the vertical stabilizers would be expected to prevent to some extent the normal loss in lift at the wing tips. The theoretical body and horizontal–tail characteristics are the same as those previously described for configuration I, as the geometry of these components are the same for the two arrangements. Since the outermost portions of the wing and the root sections of the tail surfaces are within the relatively thick boundary layer at the rear of the bodies, a reduction in lift in these regions would be expected. As an estimate of the possible magnitude of these effects, the portion of the wing and tail areas bounded by lines extending rearward from the leading

edges of the wing- and tail-body junctures were assumed to be blanketed by the body boundary layer and hence ineffective in lift. It was found that such a reduction in the effective lifting-surface area changes the theoretical lift-curve slope $dC_L/d\alpha$ and moment-curve slope dC_m/dC_L to 0.034 per degree and -0.22, respectively, which are in closer agreement with the experimental results.

Configuration III.- The results for the triangular-wing configuration (fig. 9(c)) show that the lift curve is linear throughout the angle-of-attack range and that a small negative lift coefficient exists at zero angle of attack. The pitching-moment curve indicates positive longitudinal stability which increases slightly with increasing angle of attack. The lift-curve slope $dC_L/d\alpha$ and moment-curve slope dC_m/dC_L are both somewhat less than the corresponding theoretical values. (See table II.)

The theoretical lift and pitching-moment characteristics for the wing-body combination were computed essentially by the method of reference 7. However, since this theory is applicable only to very slender wing-body combinations, it was modified because the assumption of aerodynamic slenderness is not suitable for configuration III at a Mach number of 2.0. The correction factor for the winged portion of the combination was taken as the ratio of the predictions of reference 4 to those of reference 8 at the same value of the ratio of the tangent of the semi-apex angle to that of the Mach angle. In the application of this method to the present case, it was necessary to assume that the body was cylindrical to the wing trailing edge. The differences between the experimental and theoretical lift- and moment-curve slopes are possibly the result of interaction of the flow field from the engine jet and model support with that over the model since, for this configuration, a major portion of the wing is subjected to this interference. The differences between the experimental and theoretical results are in the direction indicated by these interference effects.

Comparison of results.- The lift-curve slope $dC_L/d\alpha$ for configuration I is considerably greater than those for configurations II and III, as would be expected from the theoretical characteristics of the wing plan forms involved. It is also noted that the lift-curve slope of configuration II is somewhat greater than that for configuration III. This difference arises primarily from the presence of the tail surfaces on configuration II, as these surfaces are not included in the reference wing area upon which the lift coefficient is based. In addition, a greater increment of lift coefficient is contributed by the bodies and engine for configuration II than for configuration III due to the total difference in body size and to the difference in the reference wing area. (See table I.) Other contributing factors for this difference in lift-curve slope is that for configuration III a greater percentage of the wing area is contained within the body and the wing is subject to greater lift-reducing boundary-layer effects of the body.

For all three configurations, the pitching-moment curves indicate positive static longitudinal stability about the 25-percent point of the mean aerodynamic chord and the stability for the straight-wing configuration is considerably greater than that for the swept- and triangular-wing configurations. This difference is principally the result of the relatively large tail length (distance from centroid of tail surface to the moment reference point) of configuration I, in comparison with those of configurations II and III. The difference in stability between configurations II and III, as in the case of the lift-curve slope, is essentially due to the presence of tail surfaces on configuration II.

A comparison of the drag results (fig. 9) for the three configurations shows that the minimum drag coefficient of configuration I is greater than that for configuration II (see table II) as would be expected from the theoretical pressure-drag characteristics of the two wing plan forms involved. It is also noted that the minimum drag coefficient $C_{D_{min}}$ of configuration III (0.041 based on the wing area of configuration II) is lower than the corresponding value for configuration II. This difference is believed to be primarily due to the smaller wing thickness ratio of configuration III (table I) and to a more efficient (less drag per unit body volume) volume attainment in one body rather than two. The minimum drag coefficient for the wing of configuration II would be relatively large for a swept wing as the thickness ratio of the wing section normal to the leading edge is approximately 16 percent. A further comparison of the drag results shows that the drag due to lift, as indicated by the drag-rise factor $\Delta C_D/C_L^2$, is the least for configuration I and the greatest for configuration III. (See table II.) These differences are in qualitative agreement with the theoretical wing characteristic that the drag-rise factor $\Delta C_D/C_L^2$ is an inverse function of the lift-curve slope $dC_L/d\alpha$.

The duration of flight under specified conditions of Mach number and altitude is of primary importance in the comparison of the relative merits of the various configurations from a performance standpoint. Such a comparison can be made from an examination of the lift-drag ratios of three configurations, since the endurance at a given lift coefficient and gross weight is a function of the lift-drag ratio. The variation of lift-drag ratio with lift coefficient is presented in figure 10 for the three configurations. Since these configurations are designed to support the same nominal gross weight, the lift-drag ratios of the three configurations should be compared at lift coefficients about 20 percent lower for configuration III than for configurations I and II because of the corresponding differences in wing areas. A comparison of the curves of figure 10 on this basis shows that the lift-drag ratios for configuration III throughout its test lift-coefficient range are about 12 percent greater than those for configuration II. This range of lift coefficient corresponds essentially to the design operating conditions. Configuration II exhibits lift-drag values slightly above those for configuration I in this lift-coefficient range. An extrapolation of these curves by

the relationship

$$\frac{L}{D} = \frac{C_L}{C_{D_{min}} + [(\Delta C_D/C_L{}^2)\, C_L{}^2]}$$

(where the average experimental values of $\Delta C_D/C_L{}^2$ for each configuration were used) indicates that at a lift coefficient of about 0.23 for configurations I and II and 0.19 for configuration III, the lift-drag ratios for all three configurations are essentially the same (approximately 3.2); above these lift coefficients, the lift-drag ratios for configuration I are larger than those for configuration II, which in turn are greater than those for configuration III. This reversal in the relative values of lift-drag ratio with increasing lift coefficient is the result of the inverse relationship between the experimental values of $C_{D_{min}}$ and $\Delta C_D/C_L{}^2$ for the three configurations. (See table II.) From the curves of figure 10, it is concluded that, at the low values of lift coefficient at which the test vehicle is required to operate and for a given gross weight and altitude, the triangular-wing configuration (III) would exhibit the best aerodynamic performance characteristics from a flight endurance standpoint.

Configuration IV

Force and moment characteristics in pitch.- The results for the ram-jet engine tested alone (figs. 11(a) and 12(a)) show that with an increase in the Mach number from 2.0 to 2.9 both the lift-curve slope and the stability are increased. (See table II.) These effects of Mach number are in qualitative agreement with the theoretical and experimental results for open-nose bodies of revolution with the normal shock wave inside the duct (reference 9). For the present tests, however, a conical shock diffuser was used, and also a different inlet shock-wave configuration existed at each of the test Mach numbers as shown by the schlieren photographs of figures 14 and 15. It is noted that at a Mach number of 2.0 a normal shock wave is present just ahead of the inlet lip; whereas at a Mach number of 2.9 this shock wave is apparently inside the duct and an oblique shock wave occurs at the cone break and at the inlet lip. This difference may account for some of the reduction in drag coefficient with Mach number, as the external drag would be expected to be less and the shock-wave diffuser would be more efficient (less internal drag) with the normal shock wave just inside the duct entrance.

The results for the engine, strut, and body combination (figs. 11(b) and 12(b)) show an effect of Mach number similar to that for the engine alone. That is, with increasing Mach number, the lift-curve slope and stability increase and the minimum drag coefficient decreases. The lift-curve slope of the body, as indicated by the difference between the lift-curve slope of the combination and of the engine is the same for the two

test Mach numbers, as would be expected. (See table II.) This value is also in close agreement with the theoretical lift-curve slope of the body alone, calculated on the basis of a cylindrical afterbody to account roughly for the actual flow conditions at the rear of the body. The similarity between these experimental and theoretical results indicates that the body lift-curve slope is affected very little by the presence of the engine at the rear. However, it is noted that a small negative lift coefficient exists at zero angle of attack at both Mach numbers and apparently arises from some mutual interaction between the pressure fields on the engine and body. A comparison of the pitching-moment curves for the engine (figs. 11(a) and 12(a)) with those for the engine, body, and strut (figs. 11(b) and 12(b)), show the expected forward shift of the center of pressure at both Mach numbers due to the addition of the body to the engine. The rise in the minimum drag coefficient due to the addition of the body and strut is noted to be less at a Mach number of 2.9 than at 2.0.

The results for the complete configuration (figs. 11(c) and 12(c)) show that at a Mach number of 2.0 the lift and moment curves are essentially linear; whereas at a Mach number of 2.9 both the lift- and moment-curve slopes vary somewhat with angle of attack. The variation of moment coefficient with lift coefficient for the latter case indicates that the longitudinal stability $-dC_m/dC_L$ is reduced with increasing positive or negative lift coefficients. A comparison of these results with the theoretical characteristics shows that at both Mach numbers the experimental lift-curve slope $dC_L/d\alpha$ and the average stability $-dC_m/dC_L$ are somewhat less than the corresponding theoretical values (table II). It is also noted that relatively large values of lift and moment coefficient exist at zero angle of attack. These slope differences and zero-angle values are believed to be due primarily to interference effects of the engine, particularly those from the inlet shock wave, on the wing-body pressure field. Part of the moment coefficient at zero angle of attack is due to the engine drag. The large pressure rise across the shock wave tends to reduce the lift on the upper surface of the wing, which results in a negative change in lift coefficient. This region of reduced lift occurs behind the moment reference point, producing a positive pitching-moment coefficient. It is also possible that the lift- and moment-curve slopes are reduced due to this effect, as the intensity of the shock wave may increase with increases in angle of attack. A comparison of the results for a Mach number of 2.0 with those for 2.9 indicates that the shock-wave wing interference effect on the lift characteristics decreases with increasing Mach numbers as would be expected, since the detached engine shock wave at a Mach number of 2.0 appears to be stronger than the attached shock wave at 2.9. In addition, a larger portion of the wing is influenced by the shock wave at M = 2.0 than at 2.9. This shock-wave effect is further indicated by a comparison of the lift curve at a Mach number of 2.0 with the corresponding results for configuration III (fig. 9(c)). It is seen that configuration III, for which the inlet shock wave passes entirely ahead of the wing, exhibits

a considerably greater lift-curve slope and a smaller angle of zero lift than configuration IV.

A comparison of the drag-coefficient curves (figs. 11(c) and 12(c)) indicates that the minimum drag coefficient decreases with increasing Mach number, as would be expected from the relative drag characteristics of the configuration components. As indicated previously, a part of this drag decrease probably results from a reduction in the engine internal drag with increasing Mach number. From the decrease in drag coefficient, coupled with the corresponding increase in lift-curve slope with increasing Mach number, greater values for the lift-drag ratio would be expected at a Mach number of 2.9 than at 2.0. The lift-drag ratio curves of figure 13 show that such is the case over the test lift-coefficient range. A comparison of the lift-drag results at a Mach number of 2.0 with those for configuration III (fig. 10) indicates that the lift-drag ratios of configuration IV are slightly less (about 7 percent) than those for configuration III at a given lift coefficient. This small adverse effect of the relocation of the ram-jet engine from the front to the rear of the test vehicle arises from the smaller lift-curve slope and larger minimum drag coefficient of configuration IV as compared to those for configuration III.

The effects of longitudinal-control deflection at a Mach number of 2.9 are shown in figure 12(c). These results show that the increment in both lift and moment coefficients due to control deflection is substantially constant over the test angle-of-attack range, indicating a relatively constant-control effectiveness for small deflections over the lift-coefficient range.

Force and moment characteristics in sideslip.- The results for configuration IV in sideslip at a Mach number of 2.0 (fig. 16) show that the variations of both side-force and yawing-moment coefficients with angle of sideslip are essentially linear. The slope of the yawing-moment curve $dC_n/d\beta$ indicates that this configuration possesses positive directional stability. The rolling-moment-coefficient curve shows that the dihedral effect $-dC_l/d\beta$ is slightly adverse throughout the angle-of-sideslip range despite the relatively large wing dihedral (15°). It is noted that this effect is a maximum near zero sideslip angle, decreasing in magnitude with increasing positive or negative angles. Elimination of the adverse dihedral effect would entail some modification of the configuration such as the provision of additional wing dihedral or the redistribution of the vertical surface area such that the lateral center of pressure would be located above the vertical center-of-gravity position.

Pressure survey of body flow field.- The experimental results at zero angle of attack, indicated in figure 17, are in reasonable agreement with the theoretical results. It is noted that the effect of an angle of attack of 5° is a general reduction of the pressure level in

the flow field above the body, as would be expected. The magnitude of this effect is such that the static pressures in the vicinity of the engine inlet differ from the free-stream pressure by a maximum of only about 2.5 percent of free-stream dynamic pressure, which is only slightly greater than the maximum value for zero angle of attack. On the basis of these pressure-survey results, the deviations of the flow conditions at the ram-jet-engine inlet from free-stream conditions are considered relatively small.

CONCLUDING REMARKS

The results of supersonic wind-tunnel tests of four configurations of a supersonic ram-jet test vehicle at a Mach number of 2.0 showed that, for three low-aspect-ratio wing configurations with the ram-jet engine located forward, the aerodynamic performance characteristics, as indicated by the lift-drag ratio corresponding to flight at a given gross weight and altitude, of a triangular-wing configuration with a central body were superior to those of a swept-back wing or a rectangular wing with wing-tip bodies. Satisfactory static-longitudinal-stability characteristics were exhibited by all of these configurations.

The test results at Mach numbers of 2.0 and 2.9 for a fourth configuration, a triangular-wing central-body configuration with the ram-jet engine at the rear, indicated some loss in lift-drag ratio due to the interference effects between the engine and wing flow fields. The static-longitudinal-stability characteristics at both Mach numbers were found to be satisfactory, and the static-lateral characteristics at a Mach number of 2.0 were favorable in all respects except for a small negative dihedral effect.

Static-pressure surveys conducted in the flow field of the test vehicle body at two angles of attack and at Mach numbers of 2.0 and 2.9 indicated that the deviations of the flow conditions at the ram-jet-engine inlet from those in the free stream are relatively small.

Ames Aeronautical Laboratory,
National Advisory Committee for Aeronautics,
Moffett Field, Calif.

REFERENCES

1. Van Dyke, Milton D.: Aerodynamic Characteristics Including Scale Effect of Several Wings and Bodies Alone and in Combination at a Mach Number of 1.53. NACA RM A6K22, 1946.

2. Taylor, G. I.: Applications to Aeronautics of Ackeret's Theory of Aerofoils Moving at Speeds Greater than That of Sound. R. & M. No. 1467, British A.R.C., 1932.

3. Laitone, E. V.: The Linearized Subsonic and Supersonic Flow About Inclined Slender Bodies of Revolution. Jour. Aero. Sci., vol. 14, no. 11, Nov. 1947, pp. 631–642.

4. Stewart, H. J.: The Lift of a Delta Wing at Supersonic Speeds. Quart. of App. Math., vol. IV, no. 3, Oct. 1946, pp. 246–254.

5. Allen, H. Julian: Estimation of the Forces and Moments Acting on Inclined Bodies of Revolution of High Fineness Ratio. NACA RM A9I26, 1949.

6. Cohen, Doris: The Theoretical Lift of Flat Swept-Back Wings at Supersonic Speeds. NACA TN 1555, 1948.

7. Spreiter, John R.: Aerodynamic Properties of Slender Wing-Body Combinations at Subsonic, Transonic, and Supersonic Speeds. NACA TN 1662, 1948.

8. Jones, R. T.: Properties of Low-Aspect-Ratio Pointed Wings at Speeds Below and Above the Speed of Sound. NACA Rep. 835, 1946.

9. Brown, Clinton E., and Parker, Hermon M.: A Method for the Calculation of External Lift, Moment, and Pressure Drag of Slender Open-Nose Bodies of Revolution at Supersonic Speeds. NACA Rep. 808, 1945.

TABLE I. – MODEL DIMENSIONS

Quantity	Configuration			
	I	II	III	IV
Total wing area, square inches	11.52	11.56	13.83	13.83
Aspect ratio	2.0	1.0	1.30	1.30
Taper ratio	1.0	1.0	0	0
Leading–edge sweepback	0°	72°	72°	72°
Wing dihedral	0°	0°	0°	15°
Wing–section–thickness ratio (in stream direction)	0.050	0.050	0.033	0.033
Wing span, inches	4.80	3.40	4.24	4.24
Mean–aerodynamic–chord length, inches	2.40	3.40	4.35	4.35
Total elevon area, square inches	–	–	2.30	2.30
Total horizontal–tail area, square inches	4.32	4.32	–	–
Total vertical–tail area,[1] square inches	4.32	4.32	5.21	4.94
Maximum body diameter, inches	0.64	0.64	0.80	0.80
Vertical distance above the body center line to the estimated center of gravity, inches	–0.36	–0.28	–0.20	0.26

[1]Exclusive of the engine supporting strut.

Note: Areas are measured to the body center lines and are based on zero dihedral.

TABLE II.- SUMMARY OF RESULTS

Configuration	Reference dimensions		M	Lift		Moment		Drag		Side force	Yawing moment	Rolling moment
	S ($in.^2$)	$\bar{c}$ (in.)		$\left(\frac{dC_L}{d\alpha}\right)_{L=0}$ (per deg)	$\alpha_{L=0}$ (deg)	$\left(\frac{dC_m}{dC_L}\right)_{av}$	$C_{m_{L=0}}$	$\left(\frac{\Delta C_D}{C_L^2}\right)_{av}$	$C_{D_{min}}$	$\frac{dC_Y}{d\beta}$ (per deg)	$\frac{dC_n}{d\beta}$ (per deg)	$\frac{dC_l}{d\beta}$ (per deg)
I	11.52	2.40	2.0	0.052 (.051)	0.5	−0.45 (−.44)	0.005	0.35	0.052	- - -	- - -	- - -
II	11.56	3.40	2.0	.034 (.038)	.7	−.19 (−.27)	−.003	.49	.047	- - -	- - -	- - -
III	13.83	4.35	2.0	.026 (.027)	.5	−.14 (−.18)	−.013	.69	.034	- - -	- - -	- - -
IV	13.83	4.35	2.0	.021 (.027)	1.9	−.22 (−.25)	.008	.70	.036	−0.017	0.0072	0.0004
IV	13.83	4.35	2.9	.023 (.025)	1.5	−.26 (−.28)	.009	.67	.027	- - -	- - -	- - -
IV Engine, strut, and body	13.83	4.35	2.0	.002	1.2	.32	.006	- -	.030	- - -	- - -	- - -
IV Engine, strut, and body	13.83	4.35	2.9	.004	1.0	.07	.005	- -	.021	- - -	- - -	- - -
Engine	13.83	4.35	2.0	.001	0	−.33	.005	- -	.021	- - -	- - -	- - -
Engine	13.83	4.35	2.9	.003	0	−.36	.003	- -	.017	- - -	- - -	- - -

Note: The values indicated in parentheses are the theoretical results corresponding to the experimental values directly above.

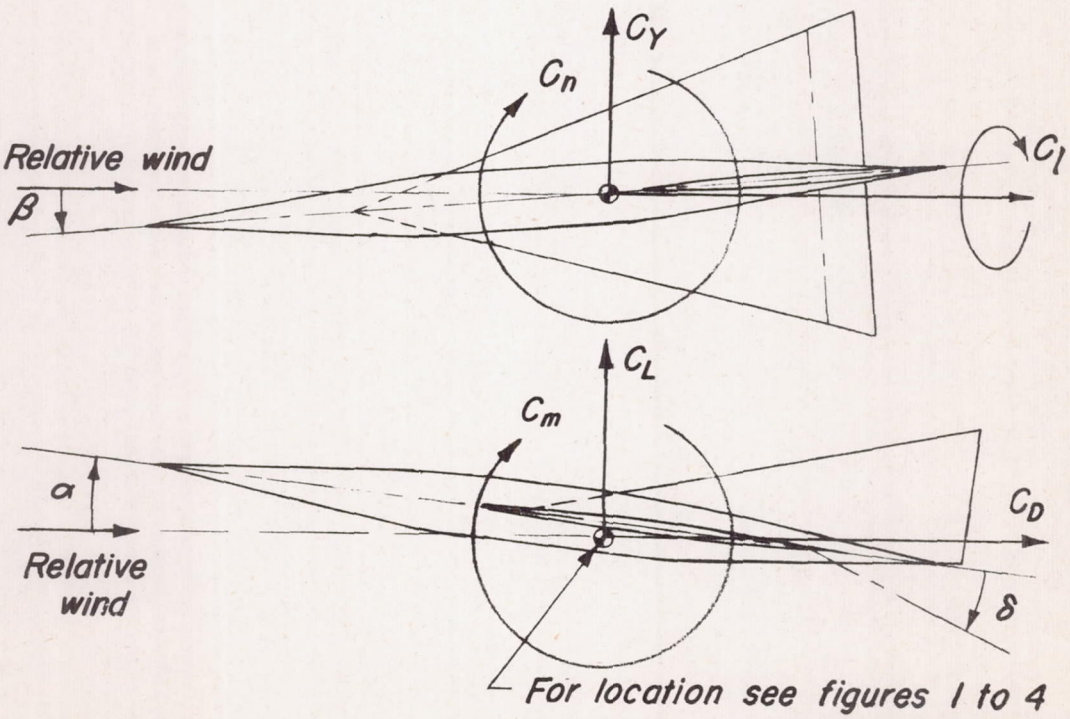

Positive directions of coefficients and angles

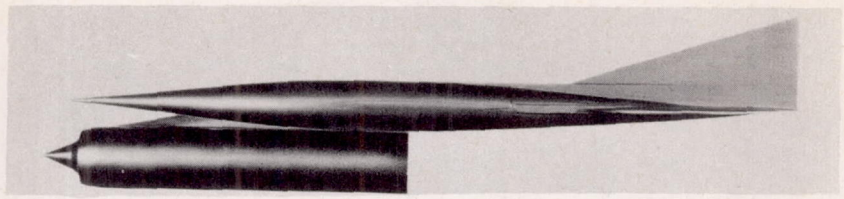

(a) Side view.

NACA
A-12869.1

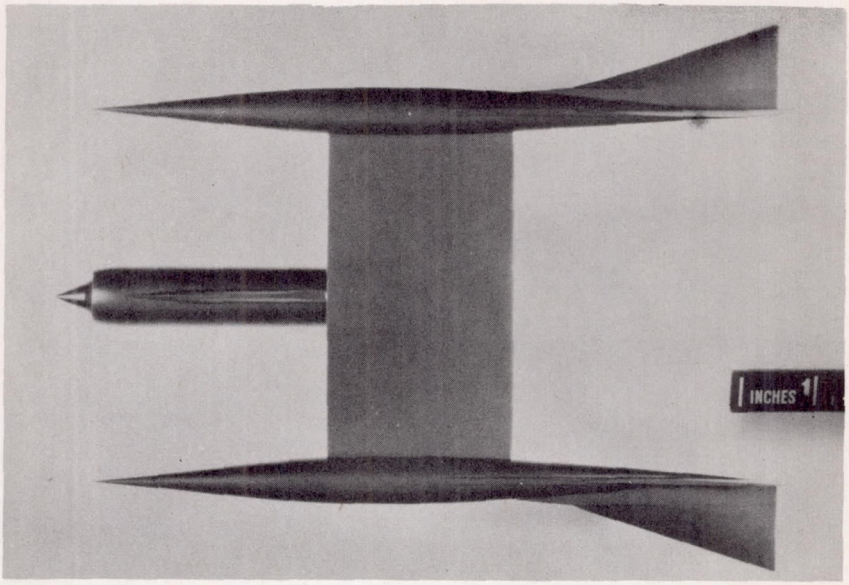

(b) Plan view.

NACA
A-12867.1

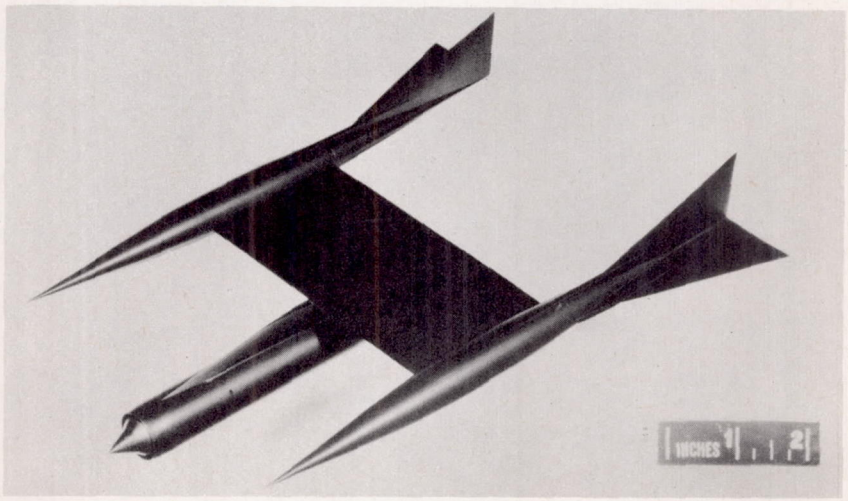

(c) Three-quarter view.

NACA
A-12870.1

Figure 1.- Configuration I.

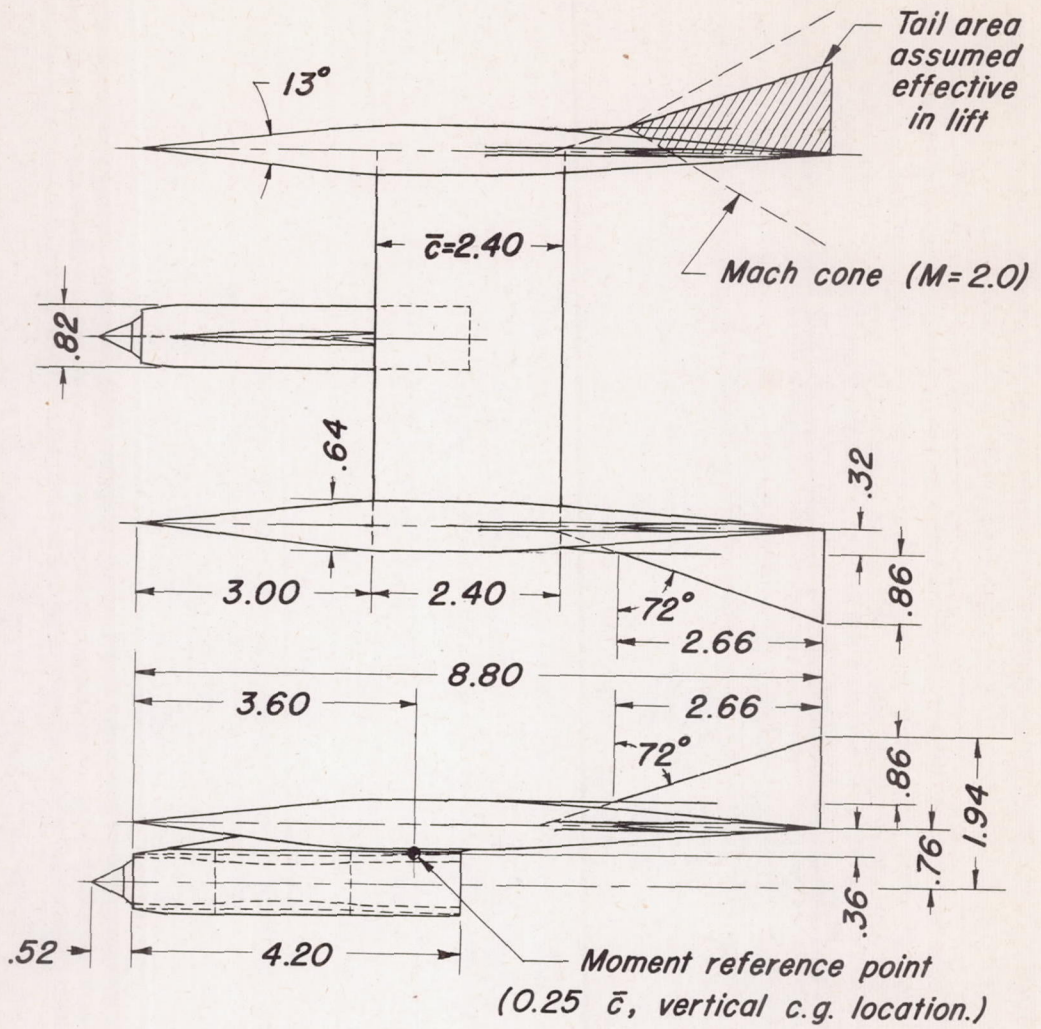

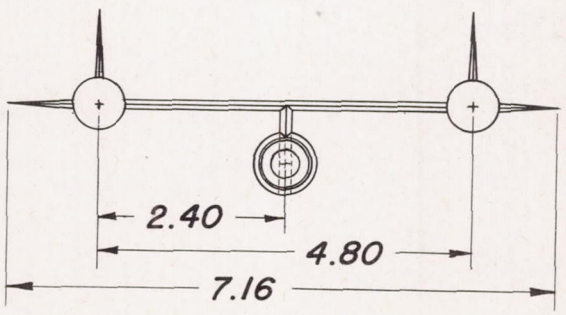

All dimensions in inches

(d) Three-view drawing.

Figure 1. — Concluded.

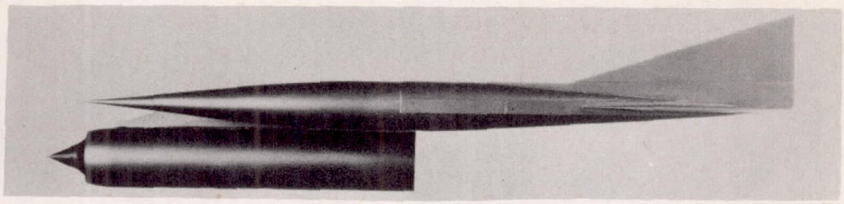

(a) Side View.

NACA
A-12878.1

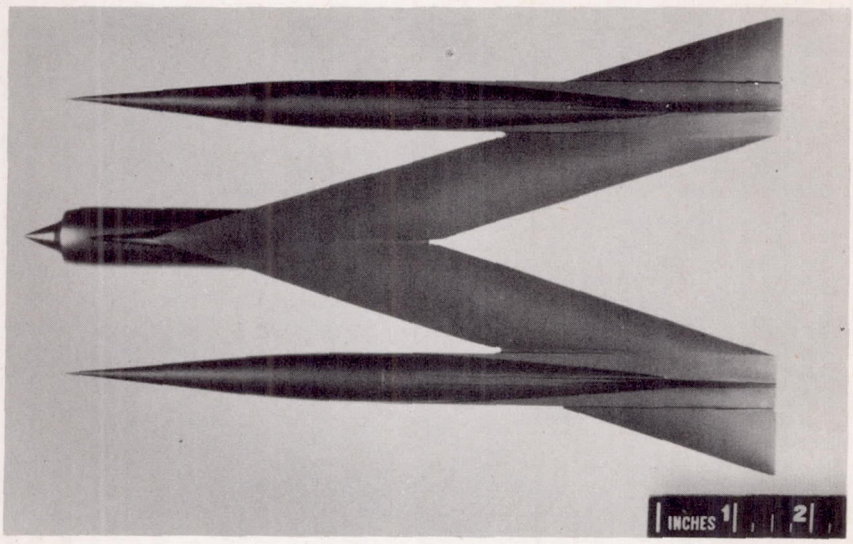

(b) Plan view.

NACA
A-12876.1

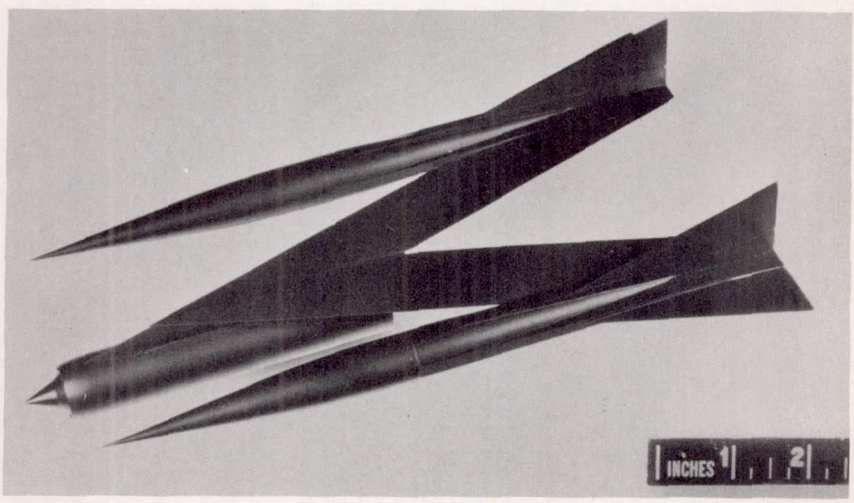

(c) Three-quarter view.

NACA
A-12879.1

Figure 2.- Configuration II.

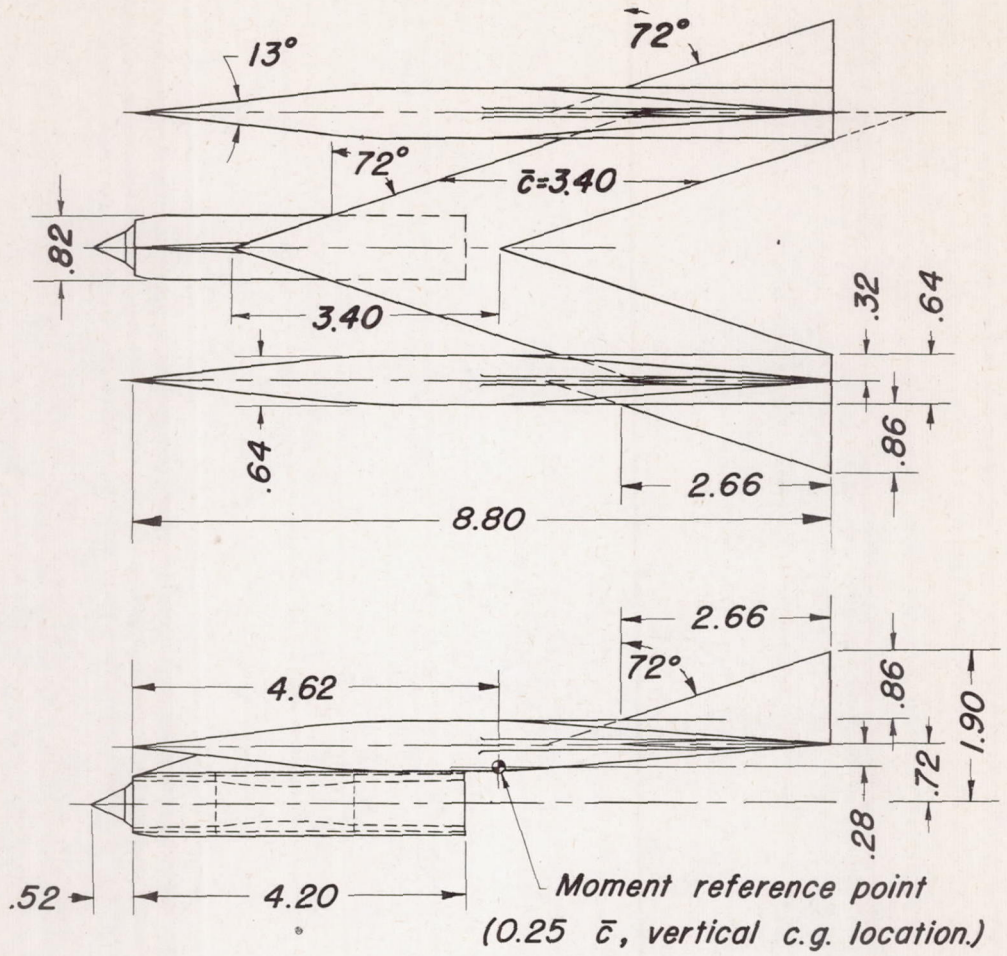

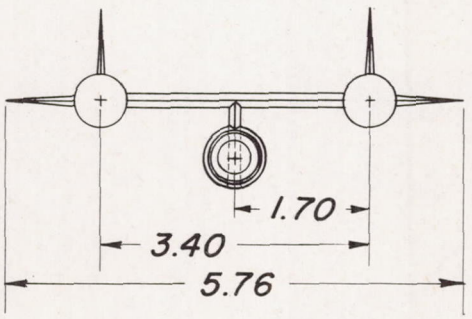

All dimensions in inches

(d) Three-view drawing.

Figure 2. — Concluded.

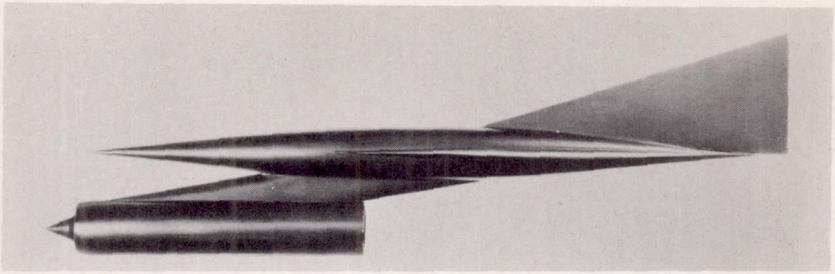

(a) Side view.

NACA
A-12864.1

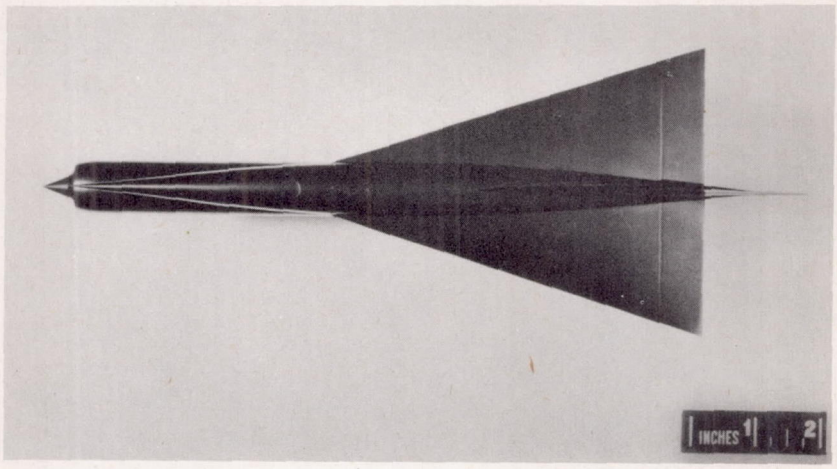

(b) Plan view.

NACA
A-12862.1

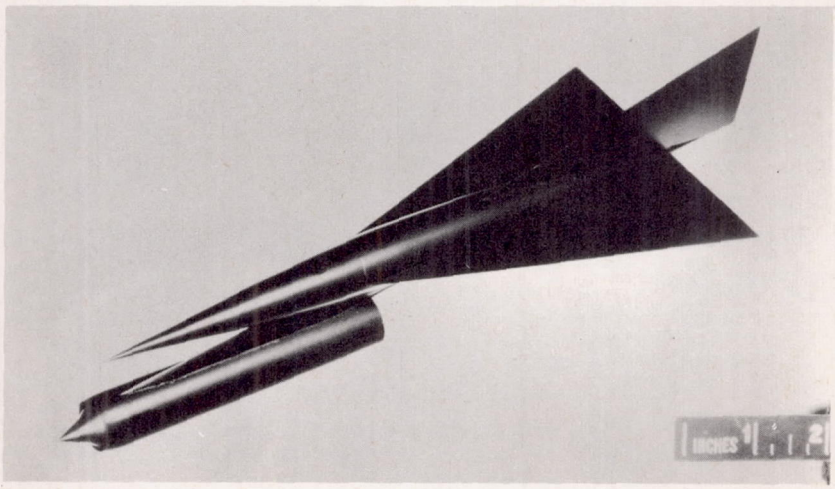

(c) Three-quarter view.

NACA
A-12865

Figure 3.- Configuration III.

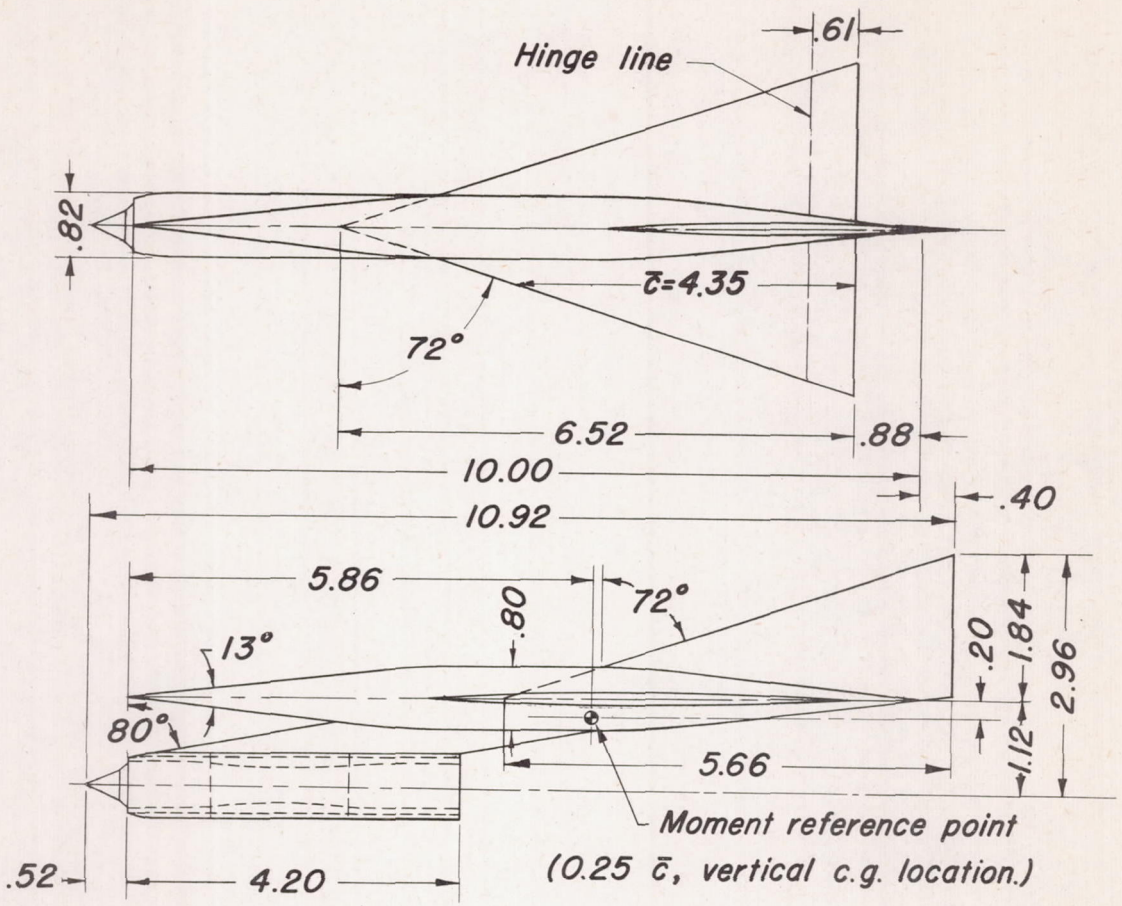

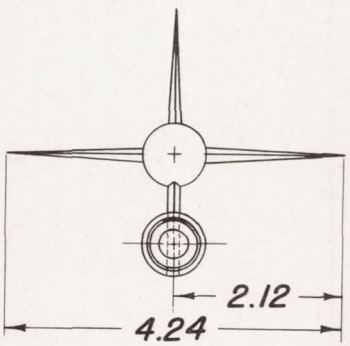

All dimensions in inches

(d) Three-view drawing.

Figure 3. — Concluded.

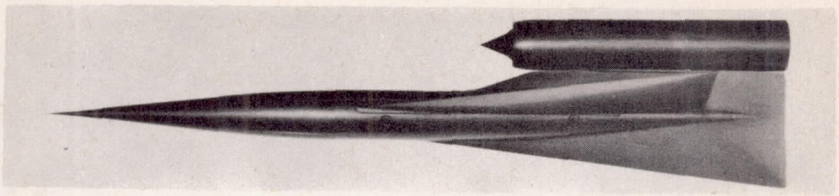

(a) Side view.

NACA
A-13237.1

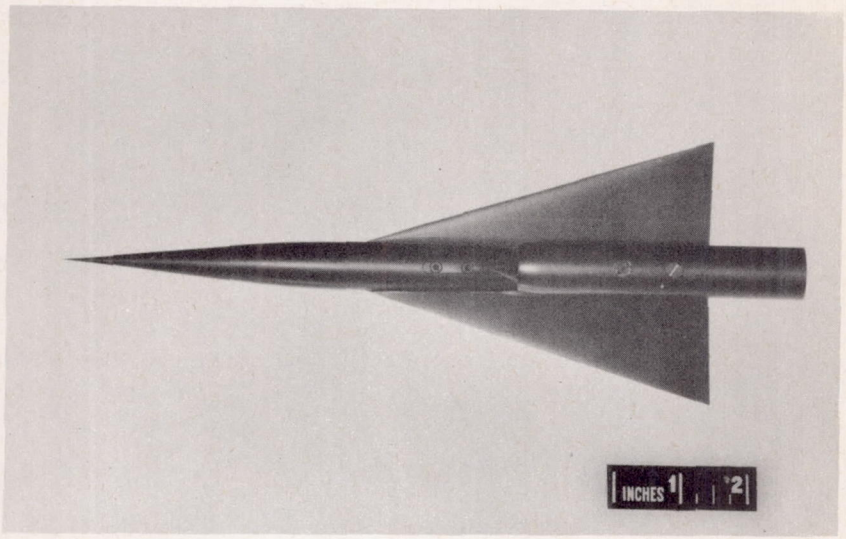

(b) Plan view.

NACA
A-13235.1

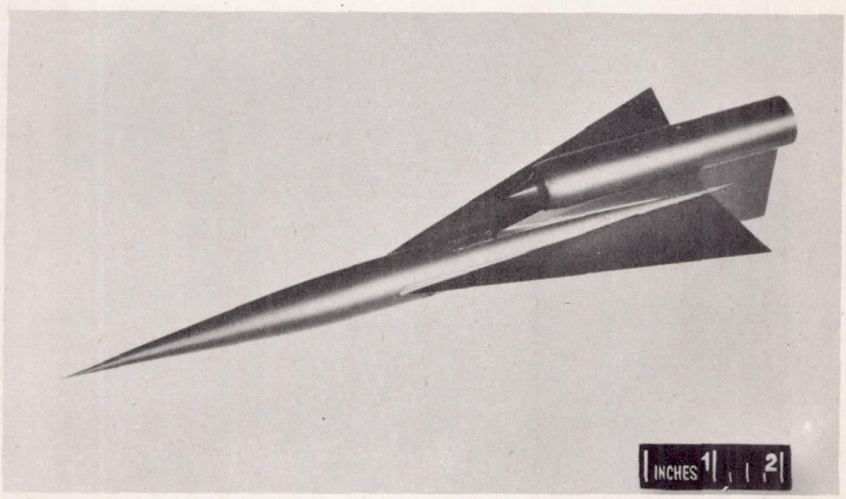

(c) Three-quarter view.

NACA
A-13238.1

Figure 4.- Configuration IV.

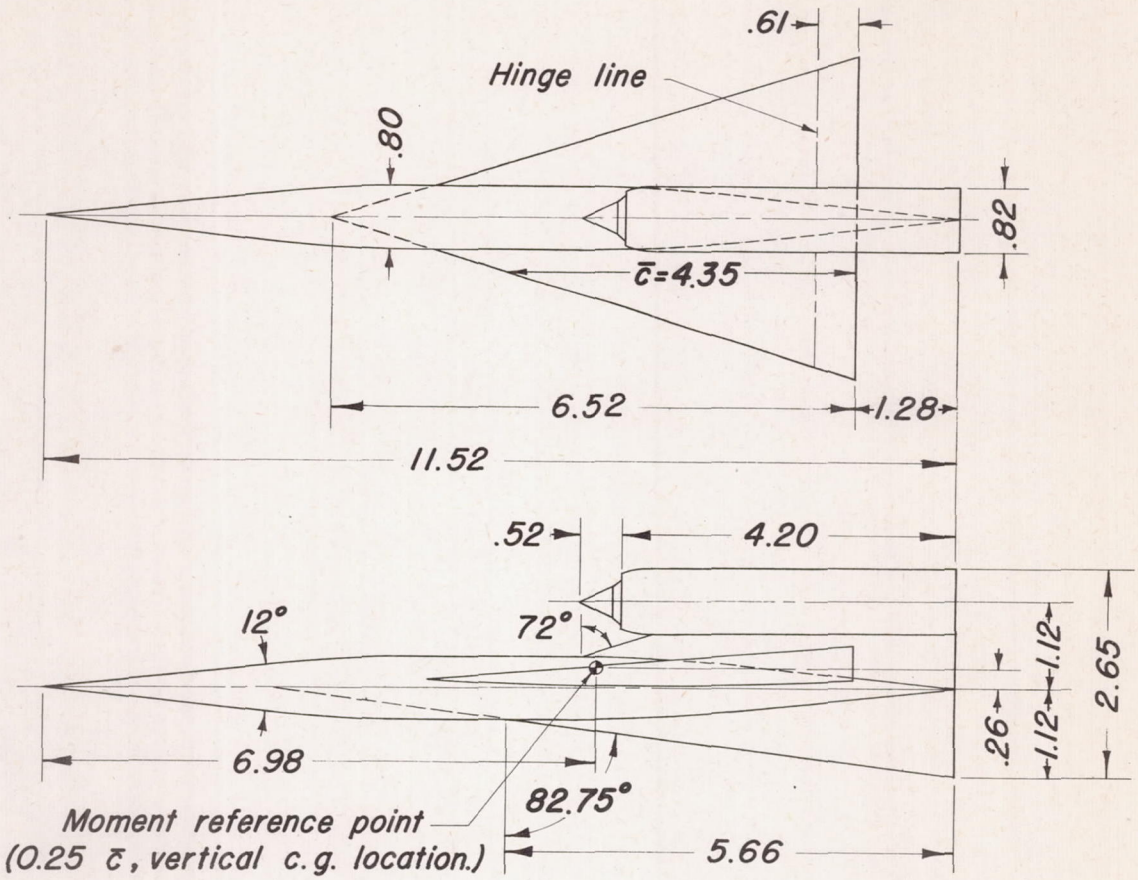

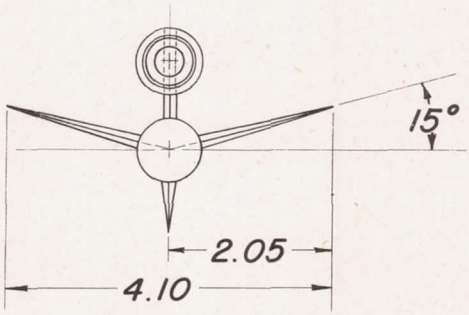

All dimensions in inches

(d) Three-view drawing.

Figure 4. — Concluded.

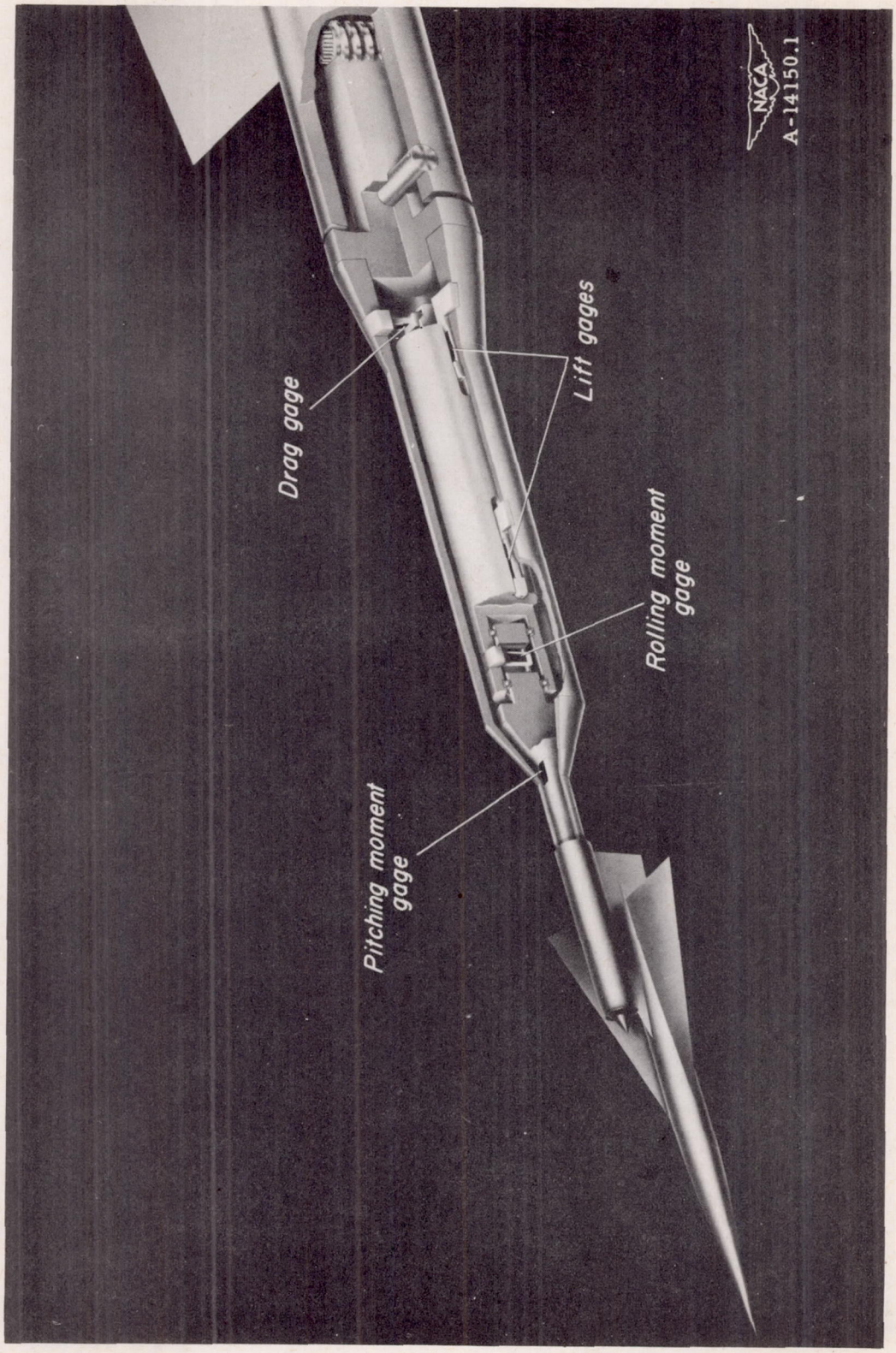

Figure 5.- Model support and strain-gage balance.

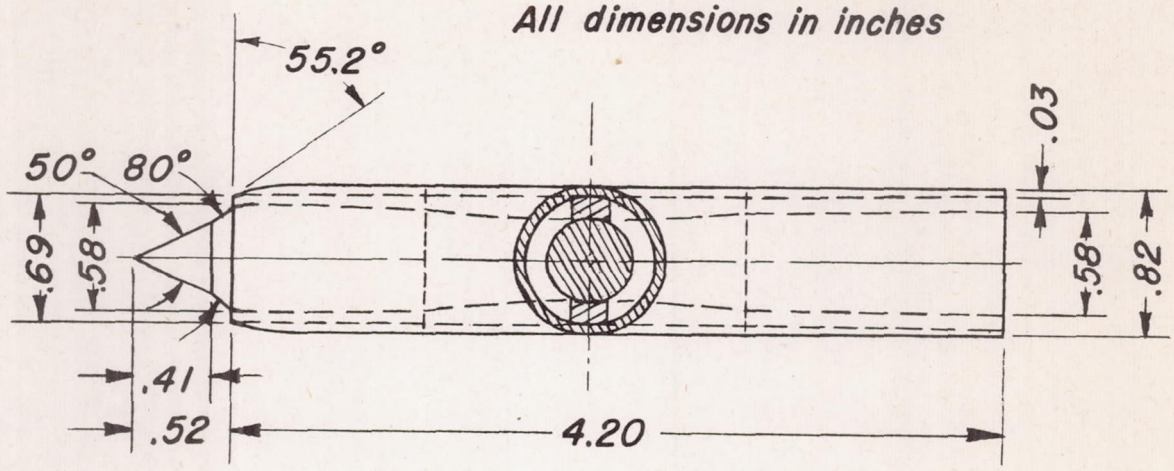

(a) External dimensions.

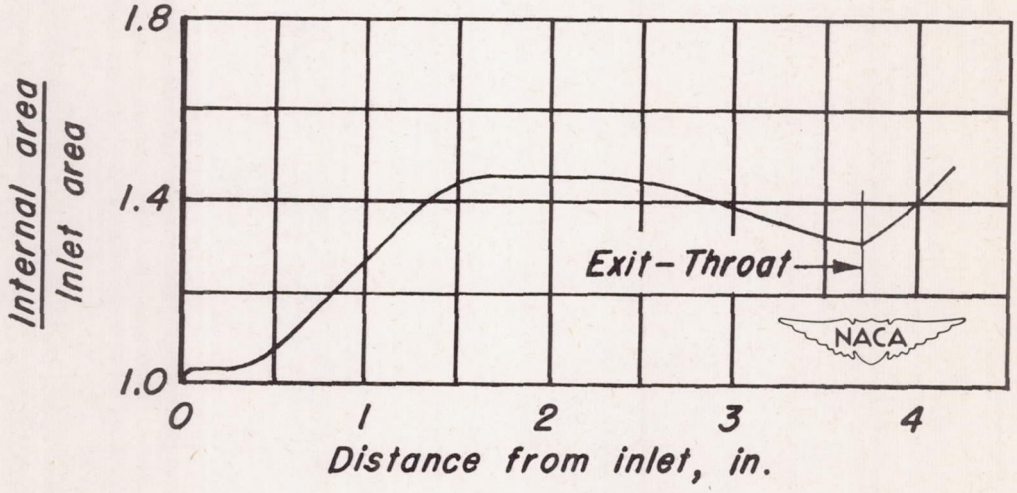

(b) Internal-area distribution.

Figure 6.- Physical characteristics of ram-jet test-engine model.

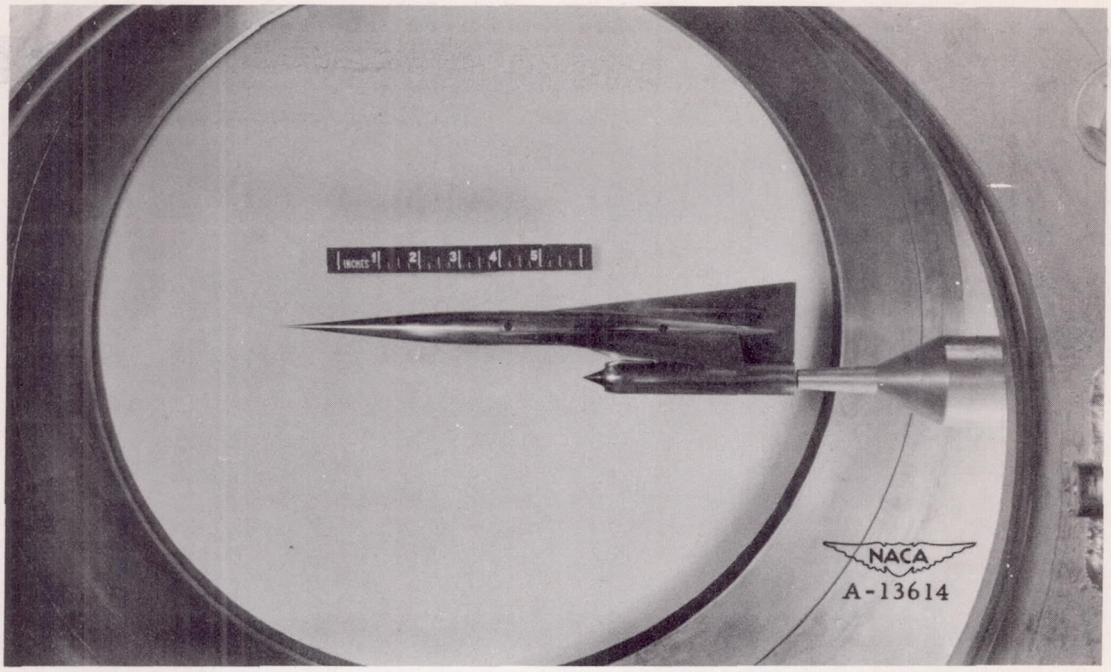

(a) Configuration IV mounted for pitch tests.

(b) Configuration IV mounted for sideslip tests.

Figure 7.- Model installations in wind tunnel.

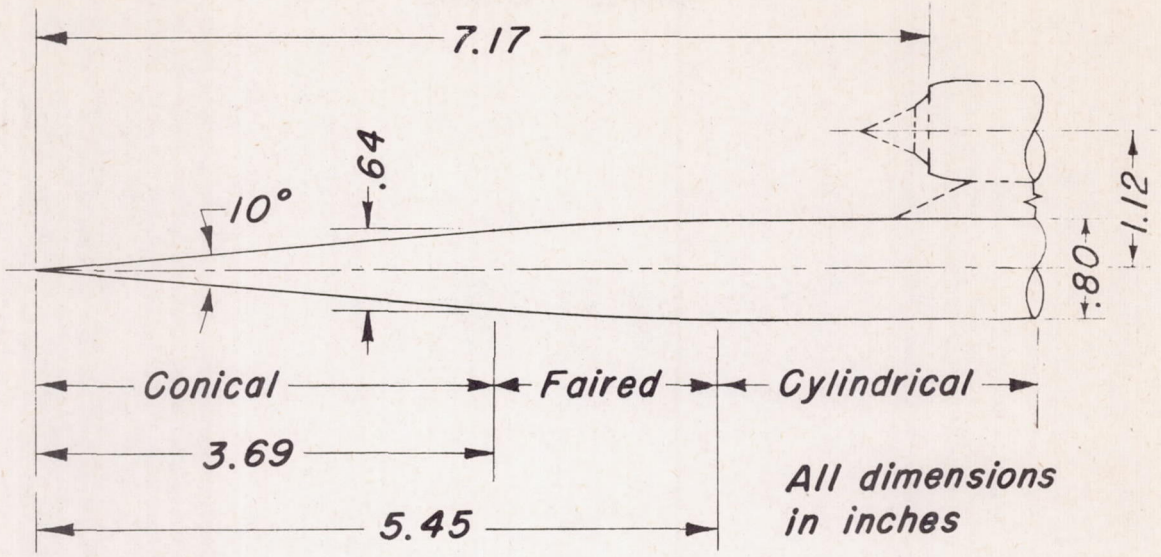

(a) Model dimensions.

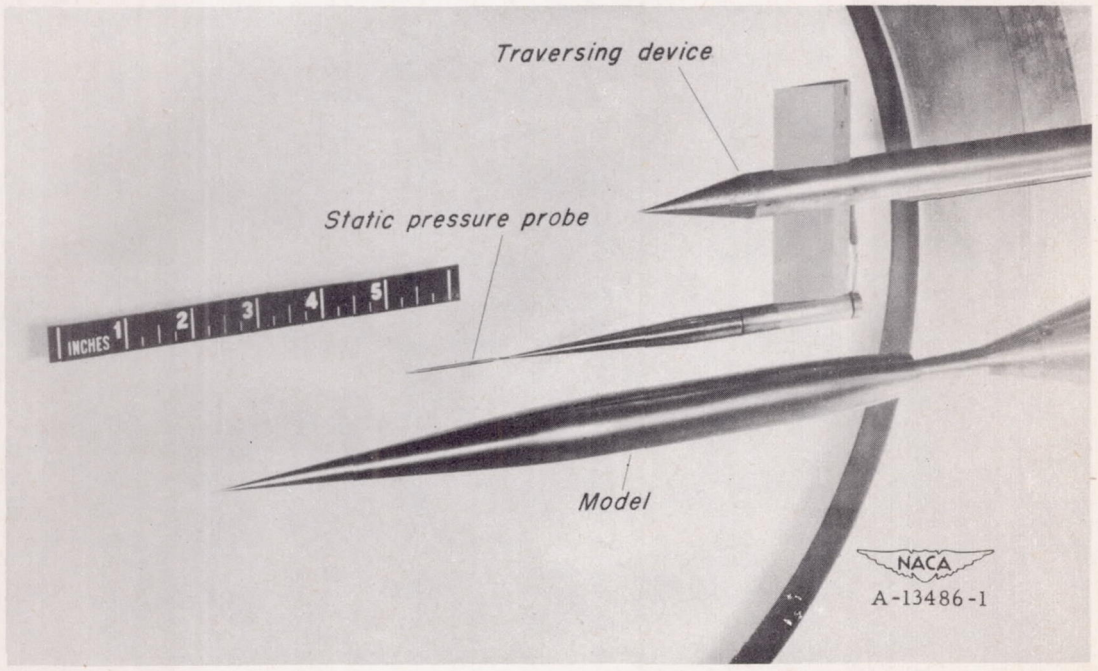

(b) Model mounted in wind tunnel with pressure survey apparatus.

Figure 8.- Body pressure survey model and installation.

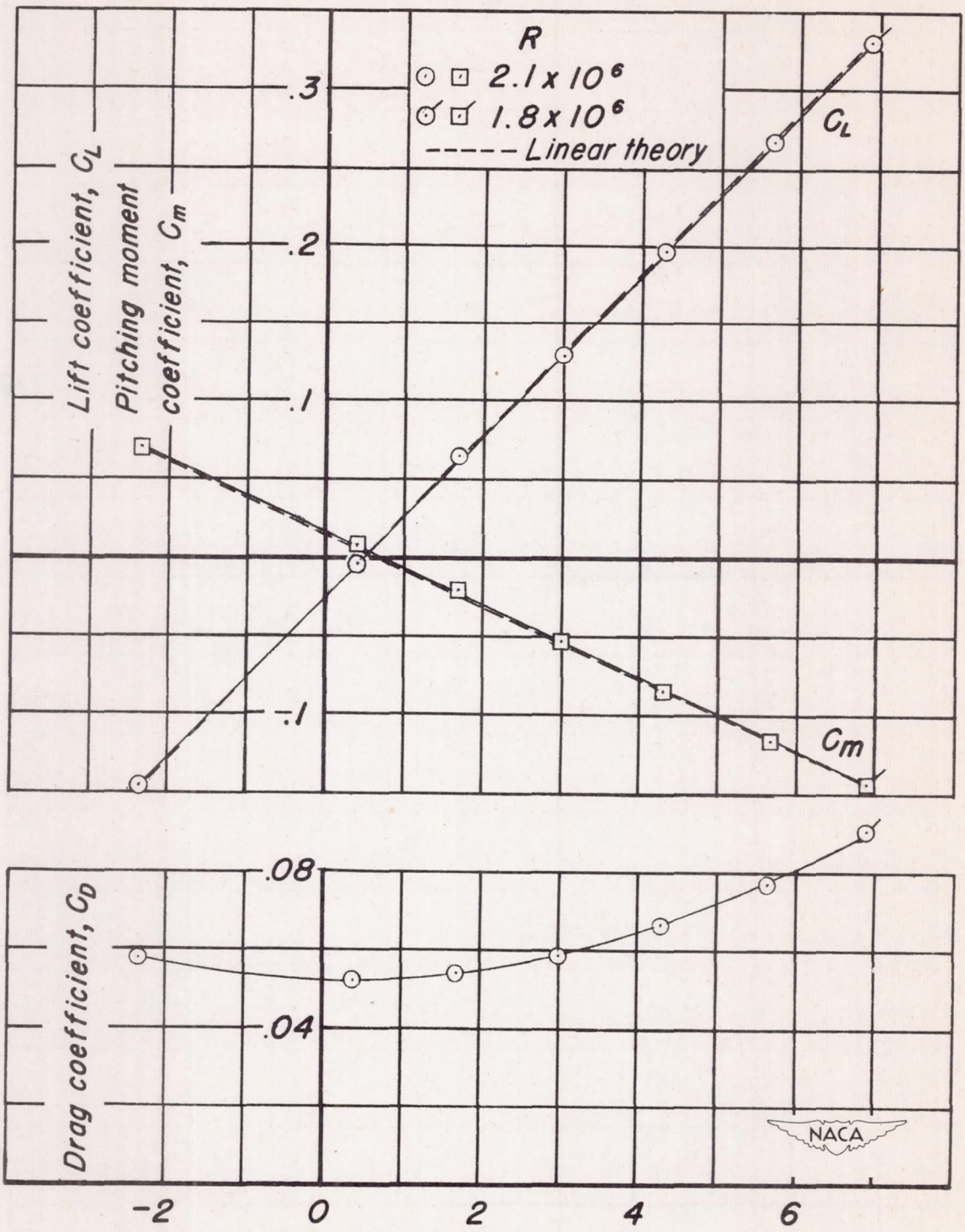

(a) Configuration I.

Figure 9.- Variation of lift, pitching-moment, and drag coefficient with angle of attack. M = 2.0.

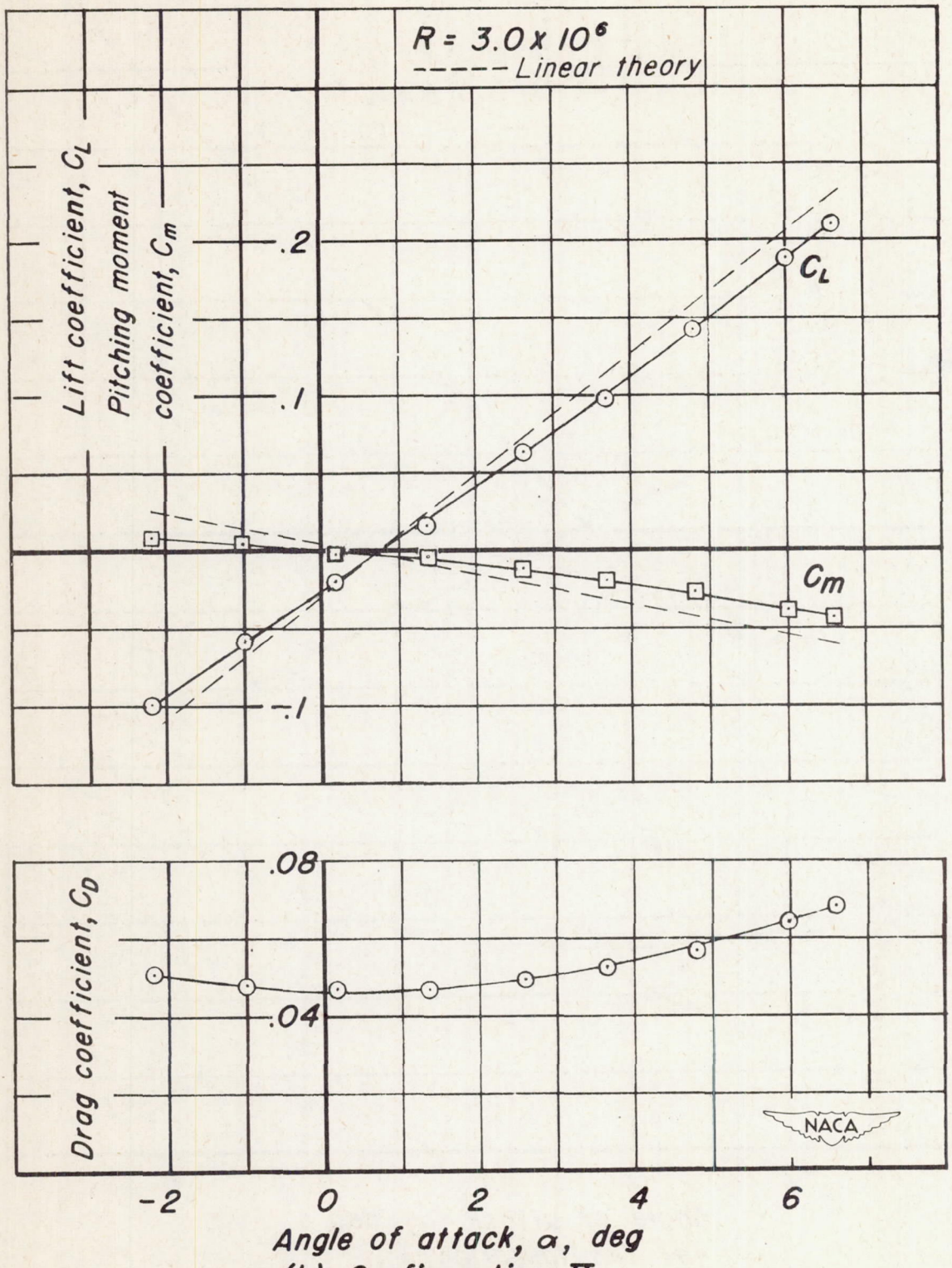

(b) Configuration II.

Figure 9.- Continued.

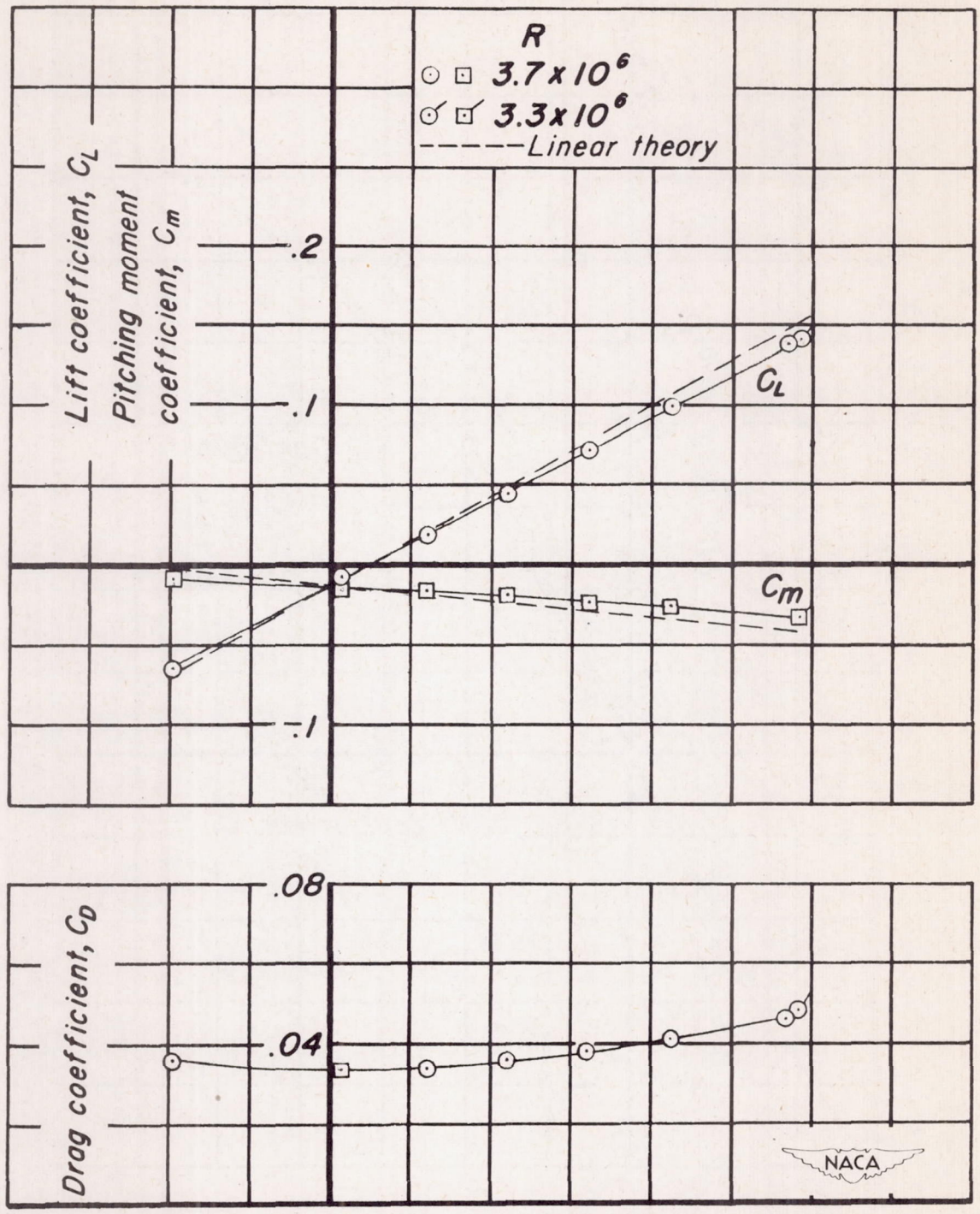

(c) Configuration III.

Figure 9.- Concluded.

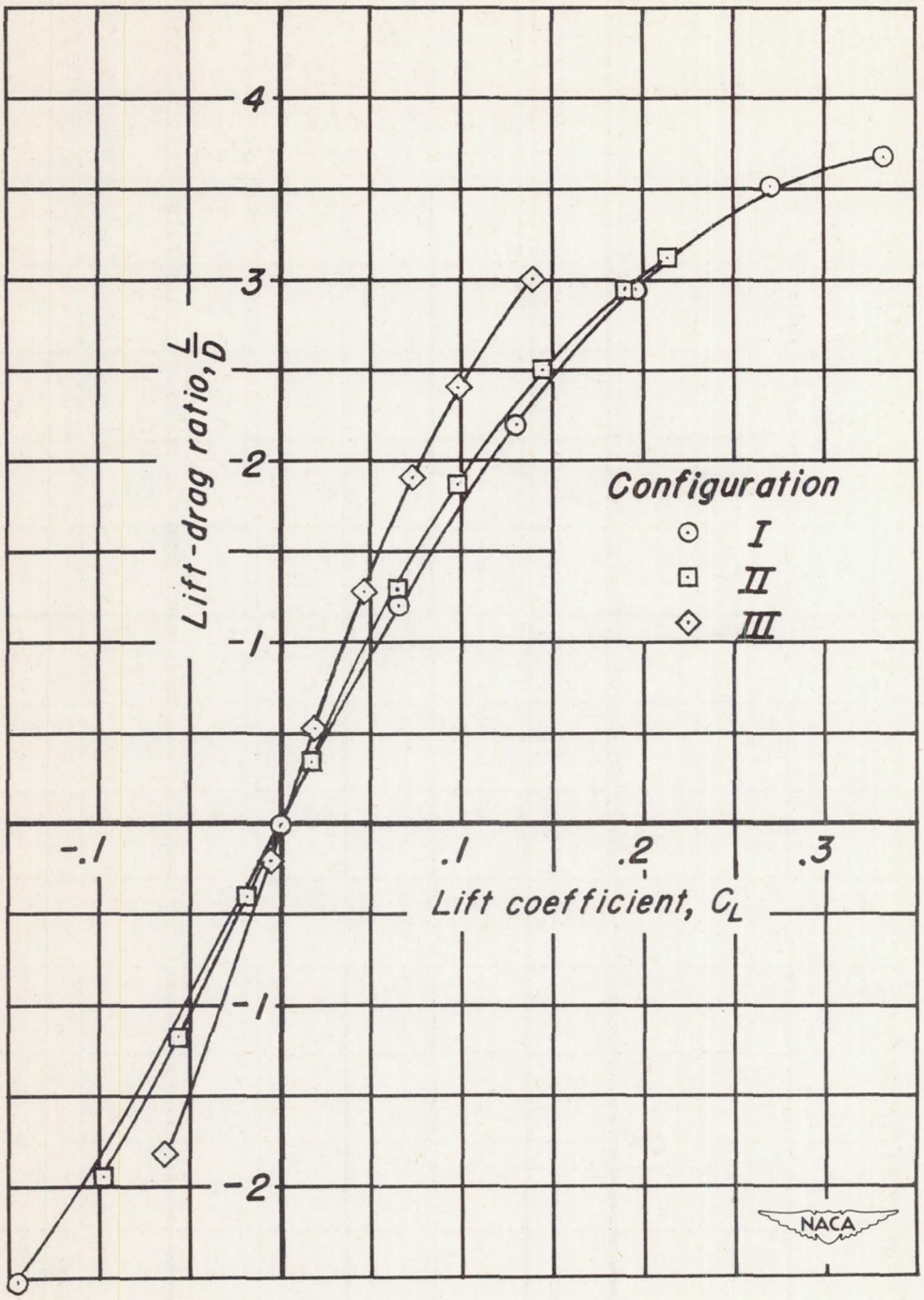

Figure 10.– Variation of lift-drag ratio with lift coefficient. M = 2.0.

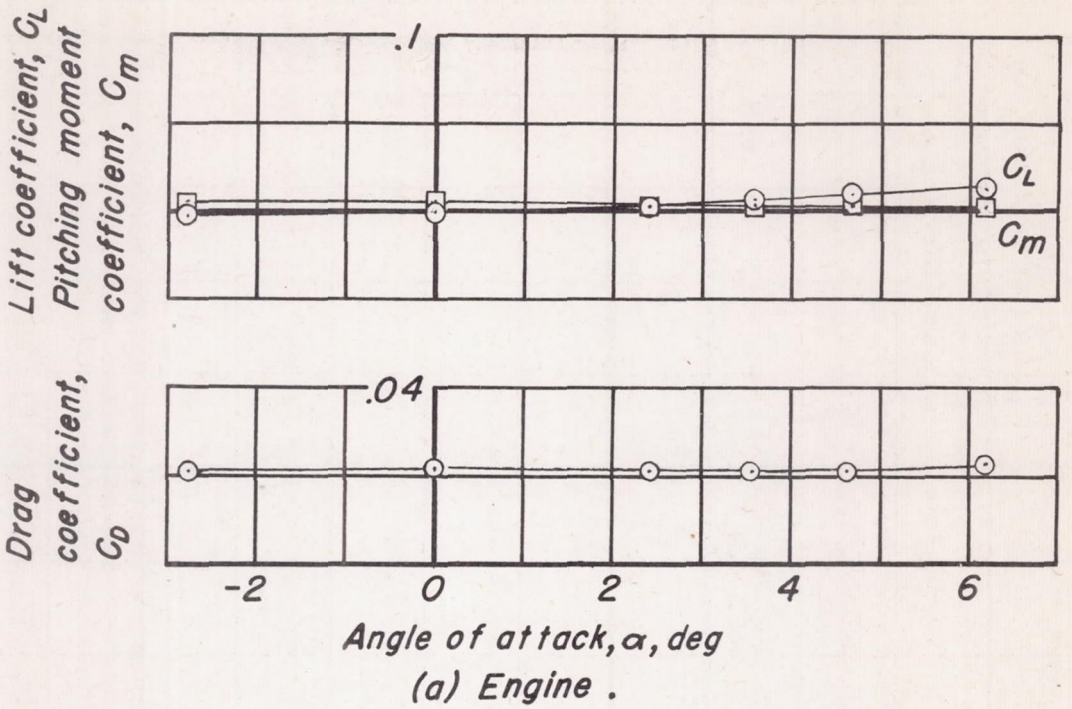

(a) Engine .

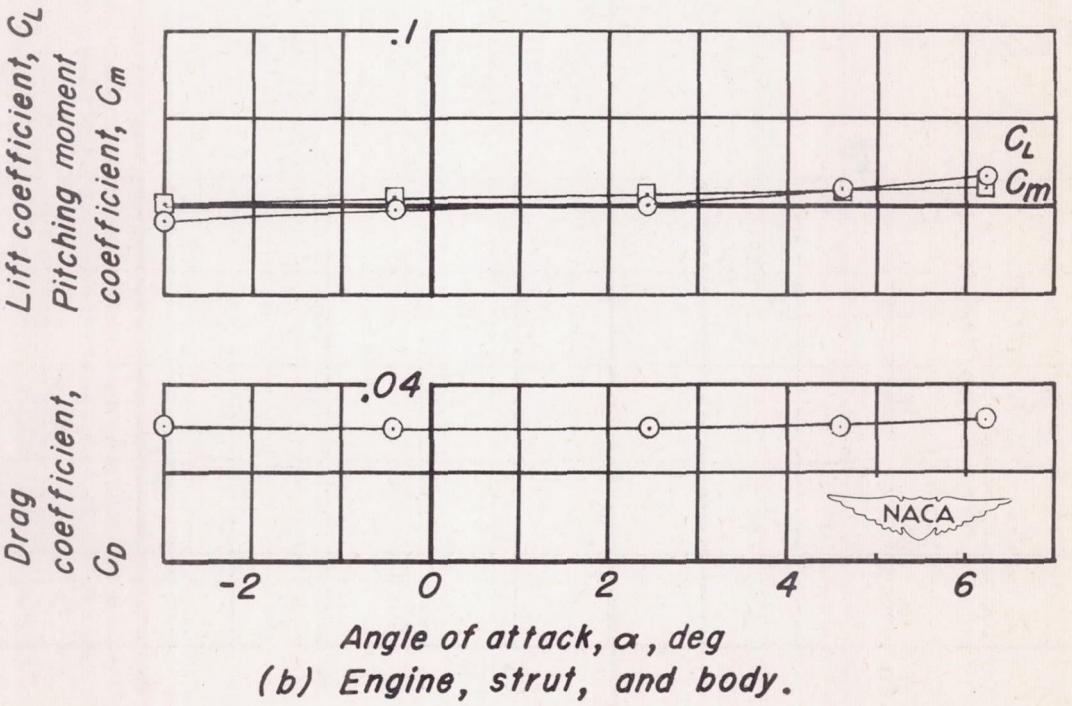

(b) Engine, strut, and body.

Figure 11 .— Variation of lift, pitching moment, and drag coefficient with angle of attack, configuration IV. M=2.0, $R=3.5\times10^6$.

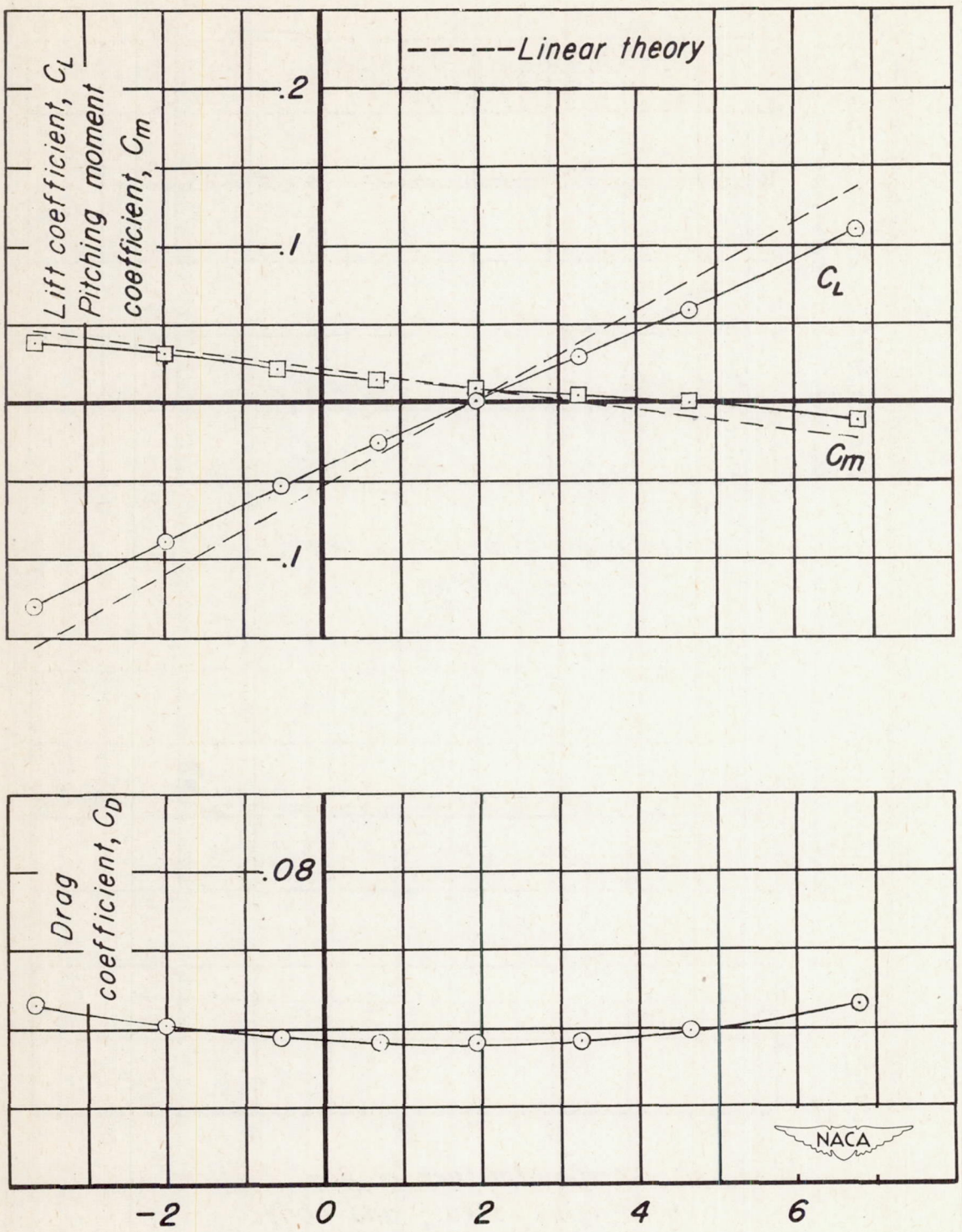

(c) Complete configuration.

Figure 11.- Concluded.

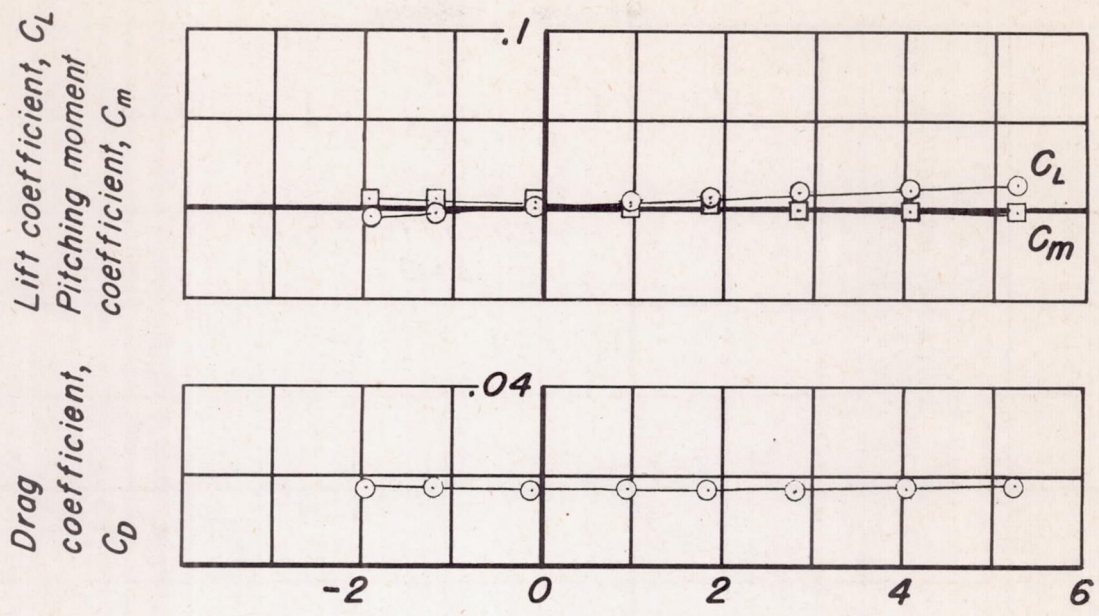

(a) Engine.

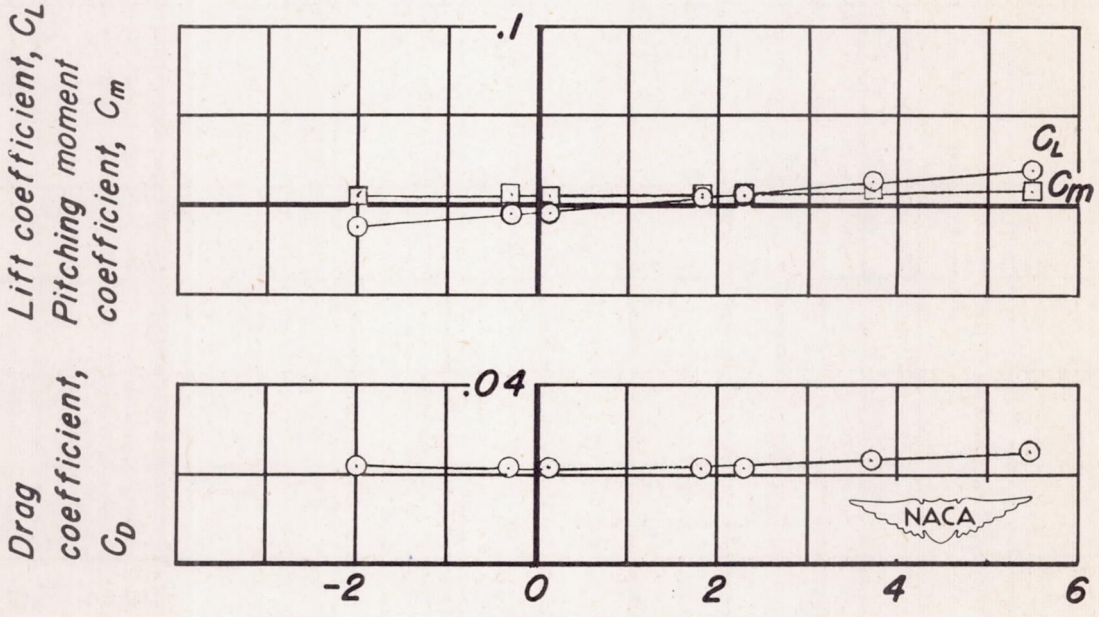

(b) Engine, strut, and body.

Figure 12. – Variation of lift, pitching moment, and drag coefficient with angle of attack, configuration IV. $M = 2.9$, $R = 5.3 \times 10^6$.

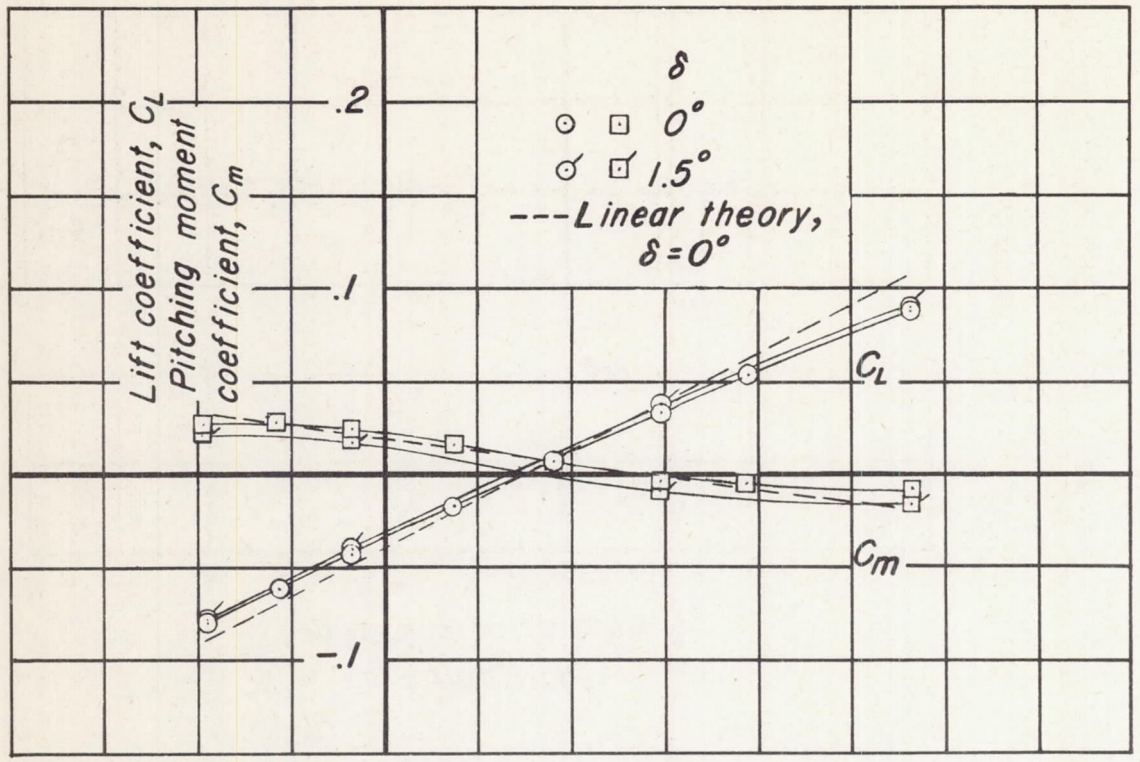

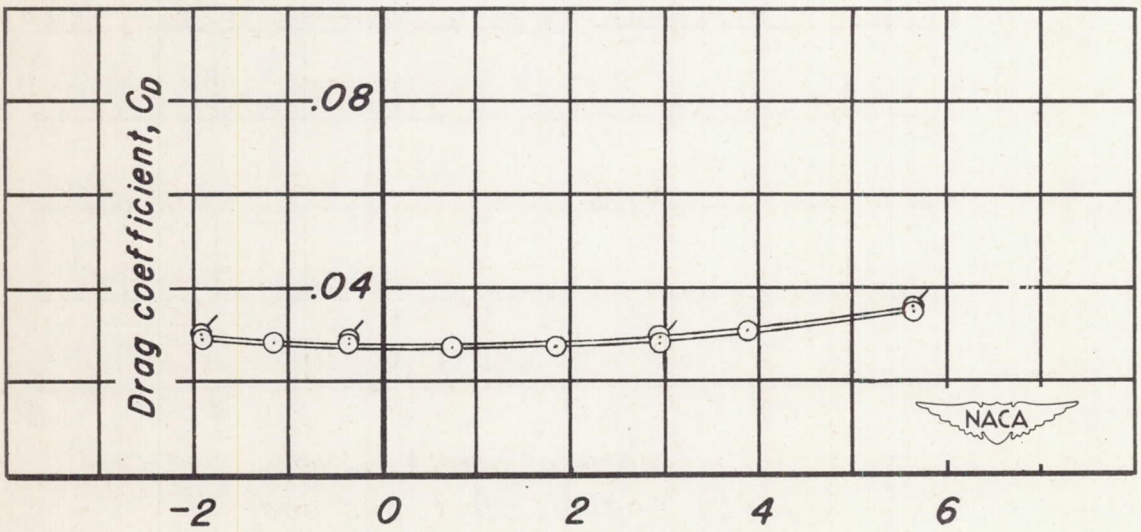

(c) Complete configuration.

Figure 12.- Concluded.

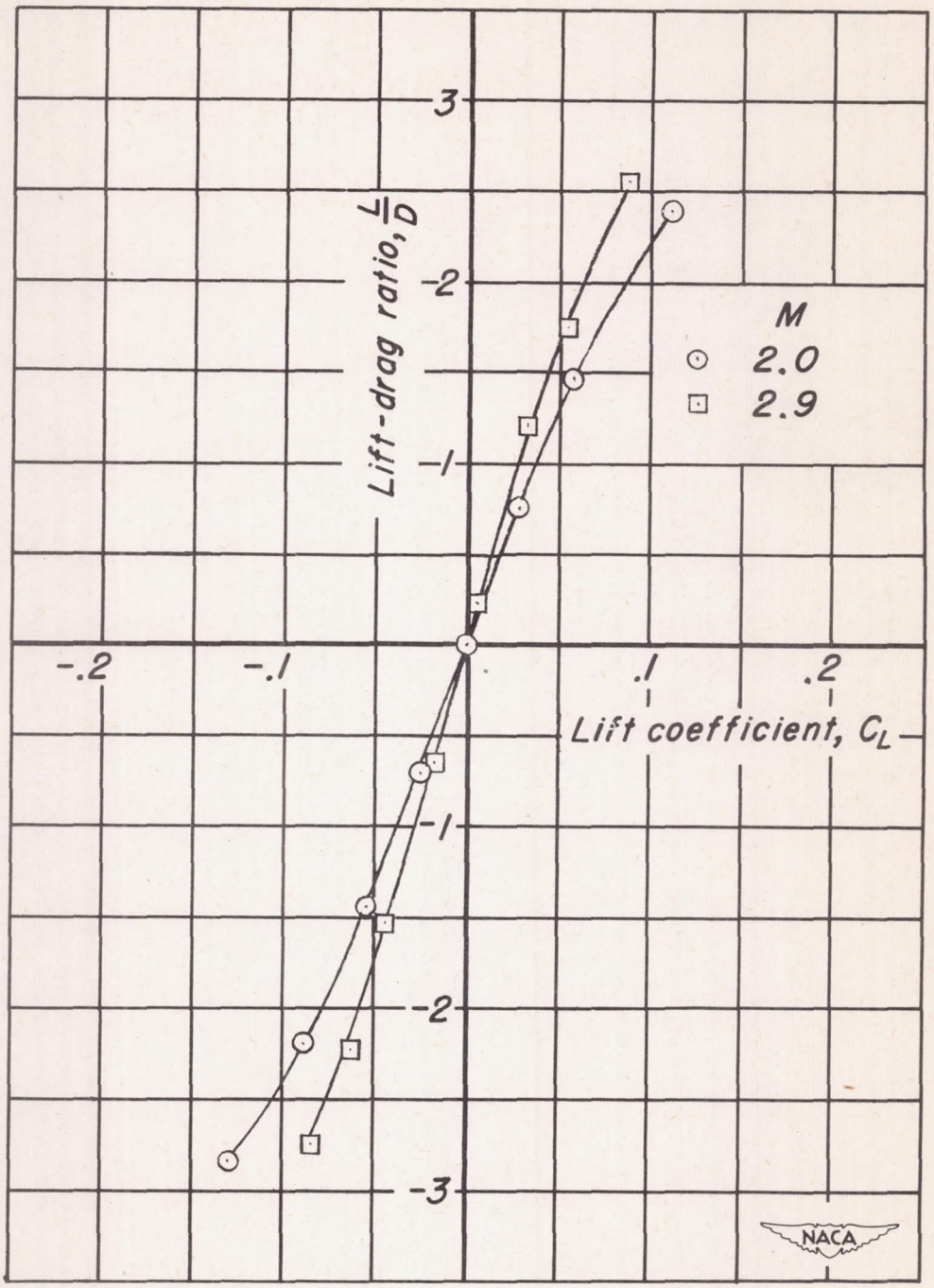

Figure 13.- Variation of lift-drag ratio with lift coefficient, configuration IV.

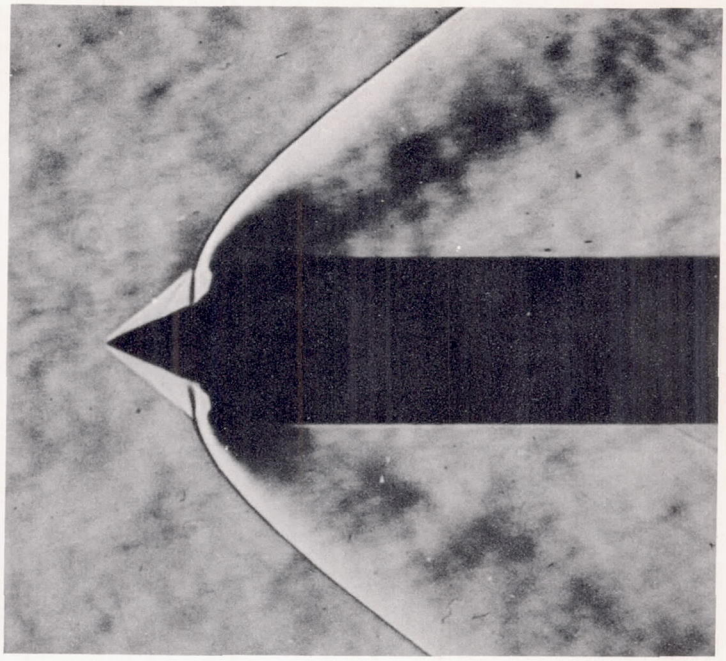

(a) $\alpha = 0^{\circ}$.

NACA
A-13704.1

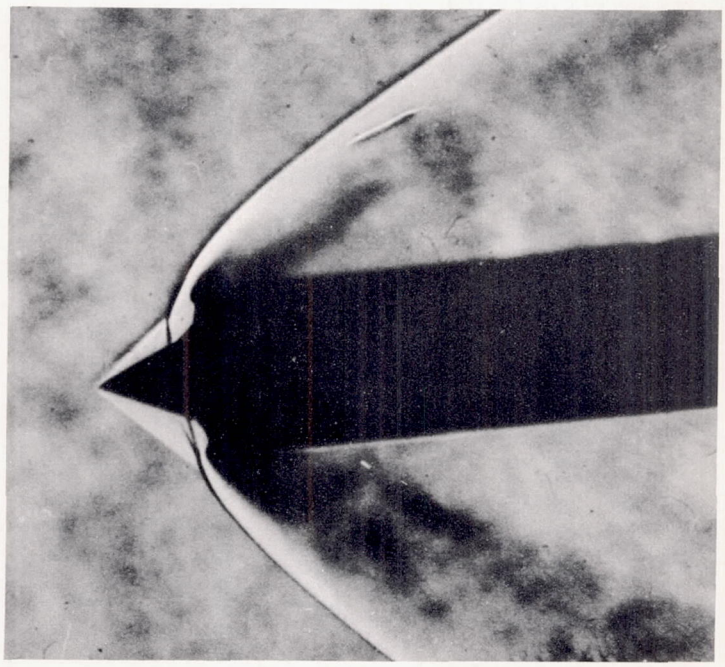

(b) $\alpha = 6.2^{\circ}$.

NACA
A-13705.1

Figure 14.— Schlieren photographs of ram-jet-engine inlet. M = 2.0.

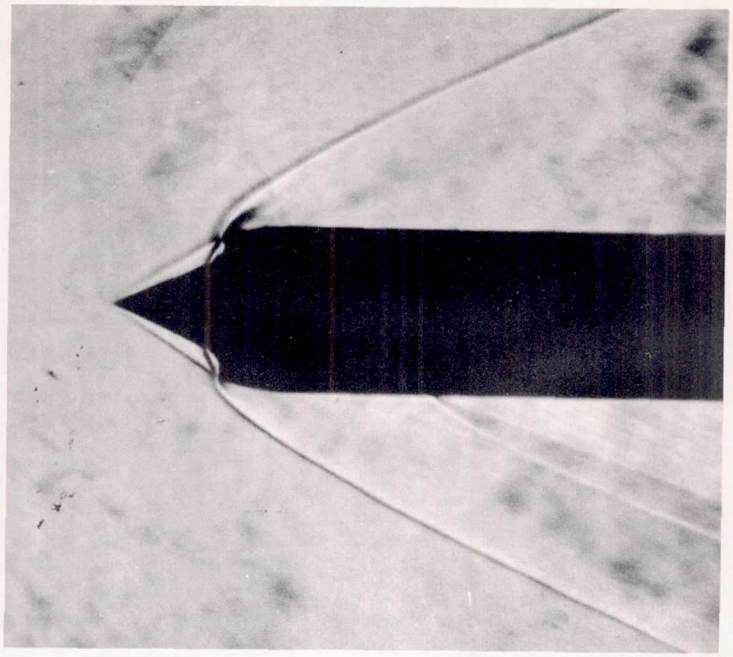

(a) $\alpha = 0^{\circ}$.

NACA
A-13905.1

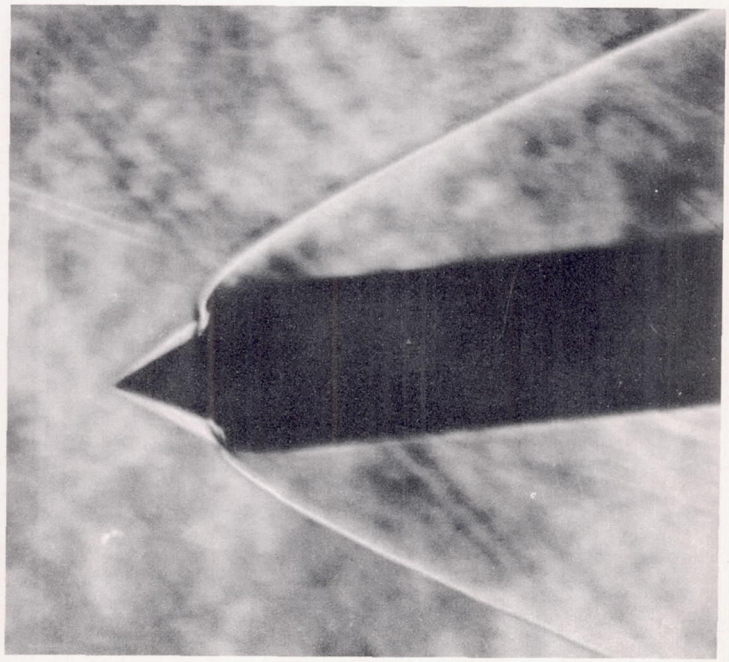

(b) $\alpha = 5.3^{\circ}$.

NACA
A-13906.1

Figure 15.– Schlieren photographs of ram-jet-engine inlet. M = 2.9.

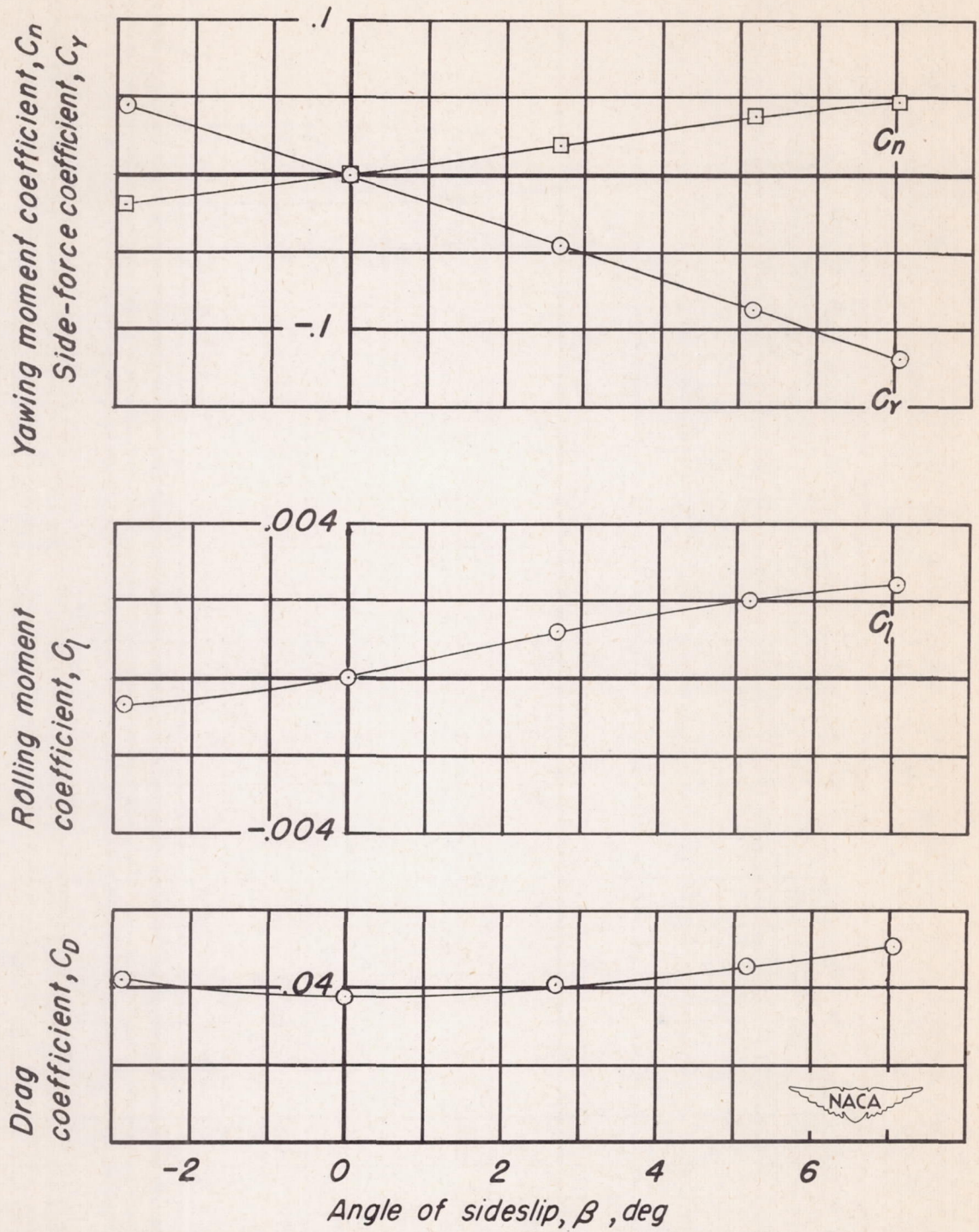

Figure 16.- Variation of side-force, yawing moment, rolling moment, and drag coefficients with angle of sideslip, configuration IV. $M = 2.0$, $R = 3.5 \times 10^6$, $\alpha = 0°$.

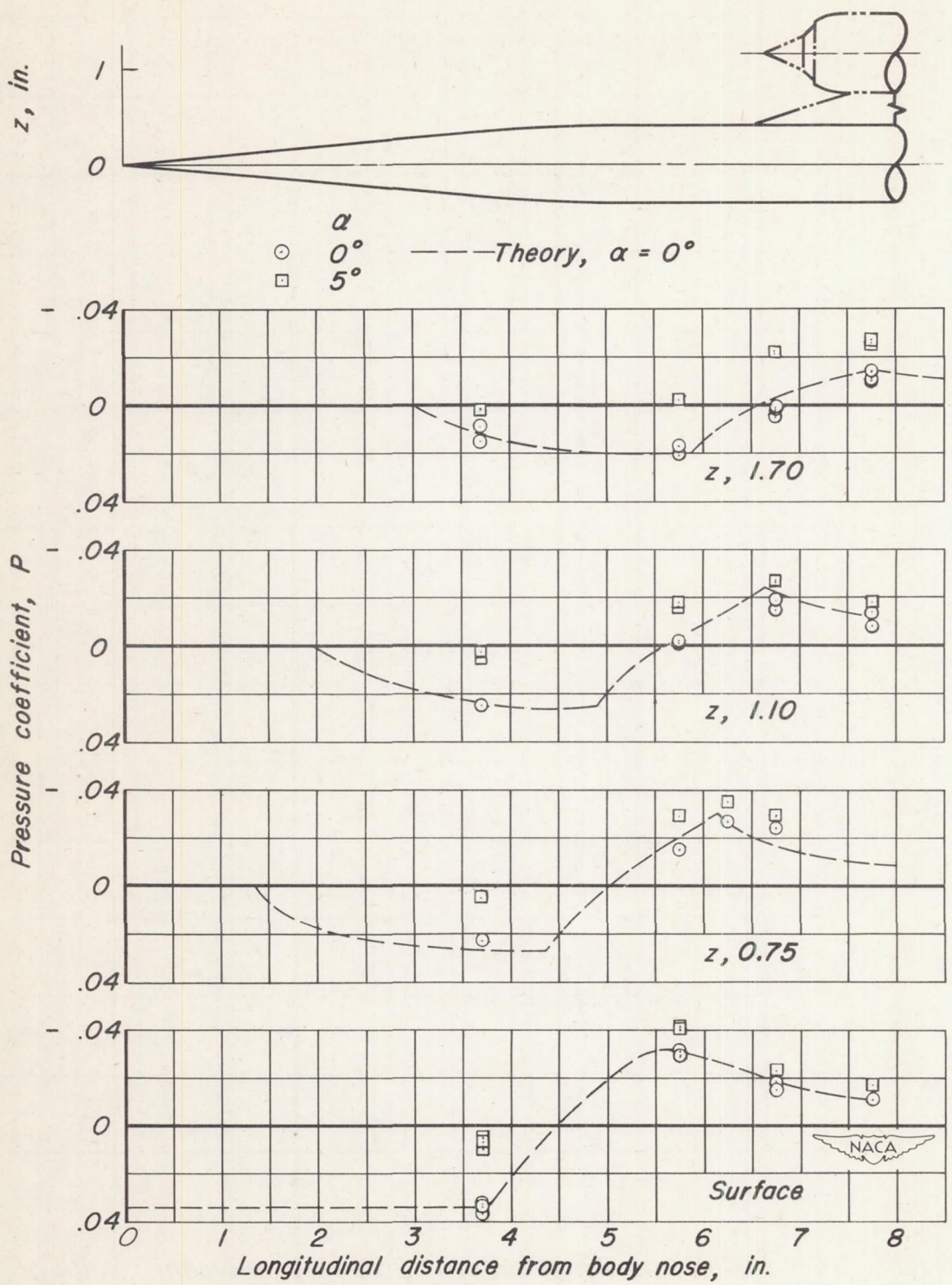

(a) M = 2.0.

Figure 17.- Pressure distribution over body.

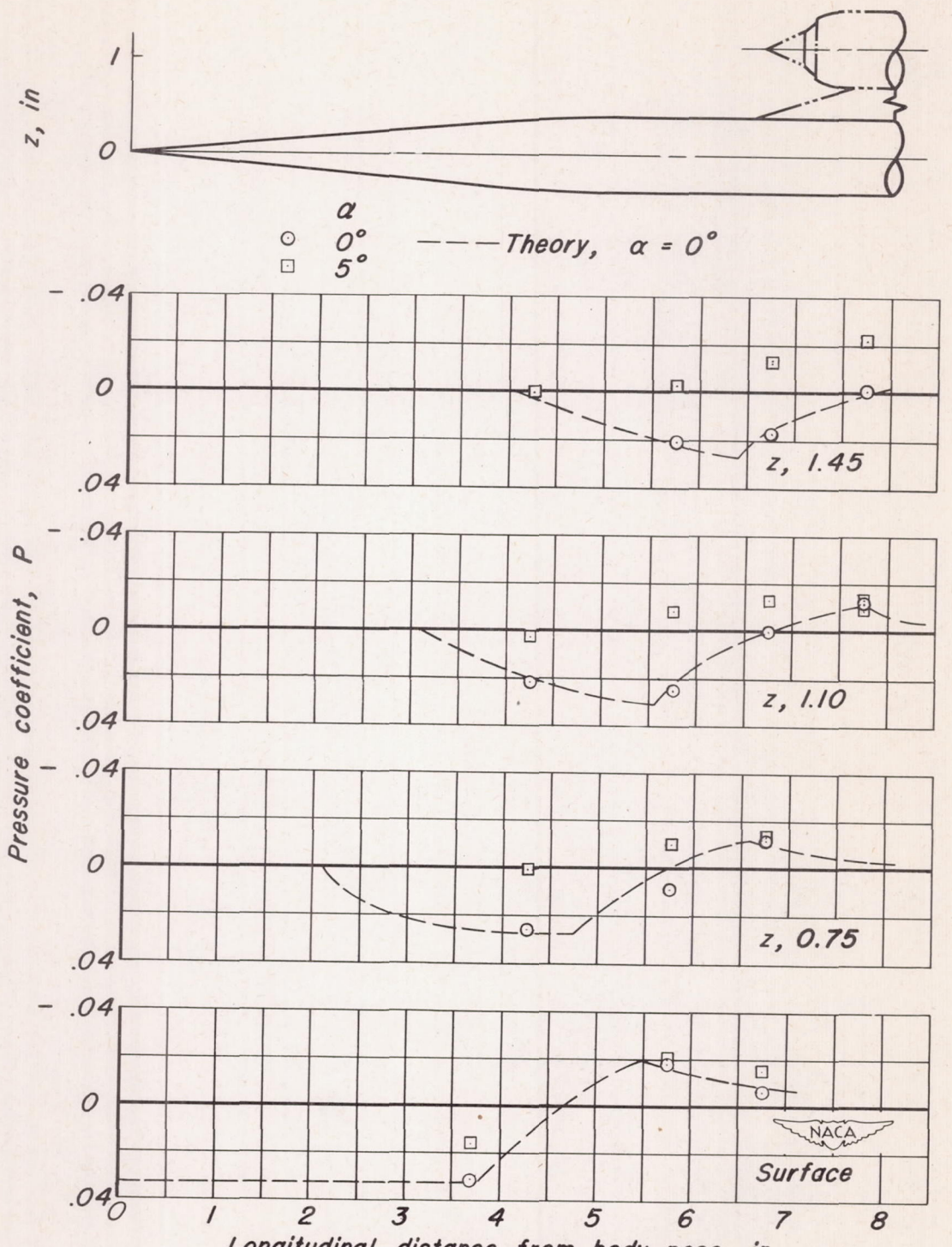

(b) M = 2.9.

Figure 17.– Concluded.

NACA-Langley - 8-18-50 - 400